https://doi.org/10.5194/egusphere-2026-5687
Preprint. Discussion started: 2 November 2026
© Author(s) 2026. CC BY 4.0 License.

Precession and meltwater control of greenhouse gas emissions from terrestrial sources during the last glacial period

Mateo Duque-Villegas[1], Thomas Kleinen[1], Victor Brovkin[1], Anne Dallmeyer[1,2], Martin Claussen[1,3], and Uwe Mikolajewicz[1]

[1]Max Planck Institute for Meteorology, Hamburg, Germany
[2]Institute of Geophysics and Meteorology, University of Cologne, Cologne, Germany
[3]Department of Earth System Sciences, Universität Hamburg, Hamburg, Germany

Correspondence: Mateo Duque-Villegas (mateo.duque@mpimet.mpg.de)

Abstract. Changing vegetation patterns in response to shifting climate over the last glacial period could explain variations in the long-term global carbon cycle, as recorded in trace greenhouse gas (GHG) concentrations in polar ice-core data. However, existing geological records provide only fragments of the vegetation cover history, and the evolution of corresponding carbon stocks and fluxes remains uncertain. Using a comprehensive Earth system model we simulate global transient trajectories of the coupled climate–vegetation–carbon system over 130 000 years of the late Quaternary, including intervals with interactive marine biogeochemistry and dynamically coupled ice sheets with iceberg calving. Our aim is to understand how vegetation changes may explain orbital and sub-orbital scale variations in the global carbon budget. According to proxy-based evidence and previous modelling applications, we find that the experiments adequately reproduce known patterns. We focus on how natural land cover transitions and productivity changes contribute to simulated terrestrial emissions of carbon dioxide (CO_2) and methane (CH_4). We classify the strength of vegetation changes and locate highly dynamic regions, found closely around monsoon margins, which respond strongly to orbital precession on a multi-millennial timescale, as well as to meltwater discharge in the North Atlantic on sub-orbital timescales. Other regions, however, respond mainly to CO_2 fertilization. During the strong meltwater pulses of the last deglaciation, in a simulation with interactive marine biogeochemistry, land biosphere changes are capable of causing marked atmospheric CO_2 jumps of close to 10 ppmv within several centuries. The simulations together highlight continental regions where interactions between shifting climate and carbon cycle components most likely contributed to GHG variability of the last glacial cycle.

1 Introduction

Natural climate fluctuations during the roughly 130 kyr (kiloyear) of the last glacial cycle occurred together with shifting vegetation patterns worldwide (Sánchez Goñi et al., 2018). In response to variable levels of seasonal warmth and moisture, atmospheric concentration of carbon dioxide (CO_2), and available ice-free land, the vegetation cover on continents changed in geographic range, composition, total biomass, and carbon (C) storage (Hoogakker et al., 2016; Nolan et al., 2018; Allen et al., 2020). Although vegetation dynamics are closely coupled with climate variability across a broad range of timescales (Fastovich et al., 2025), the sparse and discontinuous nature of geological records limits our ability to reconstruct past vegetation dynamics

https://doi.org/10.5194/egusphere-2026-5687
Preprint. Discussion started: 2 November 2026
© Author(s) 2026. CC BY 4.0 License.

globally. Therefore our understanding of the terrestrial branch of the long-term global carbon cycle remains incomplete, as demonstrated by a rather broad confidence interval in the estimated state of continental carbon inventories during full-glacial conditions (Jeltsch-Thömmes et al., 2019).

A critical uncertainty, especially in the face of ongoing accelerated environmental change, is discerning how quickly vegetation cover at the landscape scale adjusted to past climates (Harrison et al., 2025). It is still unclear whether climate and regional vegetation always tracked each other closely in time, or if they tended to stay in disequilibrium and, if so, for how long (Svenning and Sandel, 2013). In the context of glacial–interglacial climate change, palaeoecological records provide evidence for both delayed vegetation responses to climate shifts (Prentice et al., 1991; Gonzales and Grimm, 2009) as well as abrupt vegetation changes that occurred nearly synchronously with climatic transitions (Shuman et al., 2009; Williams et al., 2011; Koutsodendris et al., 2023). This variability in vegetation response times complicates the interpretation of discrepancies between model simulations and proxy-based reconstructions, such as the difference in the timing of maximum Northern Hemisphere (NH) forest cover reported by Dallmeyer et al. (2022).

For the global carbon budget during glacial cycles this means that the contribution of the terrestrial biosphere to variations in atmospheric greenhouse gases (GHG) is not fully understood (Brovkin et al., 2016). Sudden changes in vegetation cover or its productivity, as well as wildfires or abrupt permafrost degradation, are all land processes thought to explain the fast jumps in the atmospheric concentrations of carbon dioxide (CO_2) and methane (CH_4) recorded in Antarctic ice cores of the last glacial cycle (Marcott et al., 2014; Bauska et al., 2021; Riddell-Young et al., 2023, 2025; Lindgren et al., 2025). However, an incomplete global vegetation record and the complexity of interactions with marine biogeochemistry still question our understanding of the land contribution (Gottschalk et al., 2019).

Although past global vegetation patterns have been estimated from compilations of unearthed fossil plant material (e.g. Harrison, 2017; Li et al., 2025), there are still many data-sparse regions and only very few records reach as far back as, or even beyond, the Last Glacial Maximum (LGM) near 21 ka (Harrison and Prentice, 2003). As an alternative, numerical vegetation modelling in palaeo-climate contexts has provided physics-based estimates of such global patterns, and it typically captures broad features from the geological evidence (Prentice et al., 2011; Davies-Barnard et al., 2017). Yet often these approaches rely on stand-alone land-surface models forced with prescribed time slices of climate data, and they assume an equilibrium condition that neglects the role of vegetation feedbacks (e.g. Hoogakker et al., 2016; Allen et al., 2020; Huntley et al., 2023). Only a few experiments have simulated coupled climate–vegetation trajectories over glacial–interglacial cycles, but the computational cost of such interactions must be balanced with low spatial resolution in models of intermediate complexity (e.g. Ganopolski and Brovkin, 2017; Menviel et al., 2021; Duque-Villegas et al., 2022).

Modelling studies of glacial–interglacial vegetation and terrestrial carbon transitions also often ignore the role of the marine carbon cycle. Sudden changes in ocean circulation, stratification, or biogeochemistry, particularly in the Southern Ocean, are also thought to explain the fast jumps in GHG from ice-core records (Skinner et al., 2010; Ronge et al., 2021; Kobayashi et al., 2024). Because the ocean is the largest reservoir of carbon interacting with the atmosphere, it is difficult to evaluate the full

https://doi.org/10.5194/egusphere-2026-5687
Preprint. Discussion started: 2 November 2026
© Author(s) 2026. CC BY 4.0 License.

effect of land cover changes on the carbon cycle without an interactive ocean biogeochemistry, even if typical fluid and energy dynamics differ by almost an order of magnitude between land and ocean processes.

Yet another complication in studying the global carbon budget during glacial cycles is related to uncertainties in past ice-sheet evolution (Gowan et al., 2021; Bouttes et al., 2023). Glacier advance and retreat not only can push vegetation margins on mid-to-high-latitude land, but also affect global moisture and atmospheric and oceanic flows (Ganopolski and Brovkin, 2017). Indeed, simulation of climate variability in glacial-cycle transient experiments crucially depends on the choice of ice-sheet reconstruction (Kapsch et al., 2022). As a result, fast GHG variability can also emerge out of fast climate interactions with the changing cryosphere, for example from meltwater surges and subsequent abrupt cooling and warming during Heinrich events and Dansgaard-Oeschger cycles (Schannwell et al., 2024).

Our aim is to investigate how vegetation responses to last glacial cycle climate changes may have contributed to rapid atmospheric GHG variability. We are interested in the mechanisms that drive large-scale reorganizations of global vegetation patterns, and in locating regions that have the largest potential to explain rapid variations of terrestrial CO_2 and CH_4 emissions. We use a comprehensive Earth system model in a set of experiments targeting different timescales and processes. First, we evaluate the orbital influence on terrestrial processes over the glacial cycle with a 130 kyr-long transient simulation of the coupled climate–vegetation–carbon system. Second, we run a shorter experiment covering the last deglaciation only but with interactive ocean biogeochemistry to balance the contributions of terrestrial and marine processes. And third, we consider the influence of coupled cryosphere dynamics by taking into account existing data from the transient deglaciation experiments of Mikolajewicz et al. (2025). The following section explains the methodology behind the simulations and afterwards we focus on the global responses of vegetation and the carbon cycle.

2 Methods

2.1 Model description

We simulate transient dynamics of the climate–carbon system using available configurations of the coarse-resolution implementation of the Max Planck Institute for Meteorology Earth System Model (MPI-ESM) version 1.2 (Mauritsen et al., 2019; Mikolajewicz et al., 2018). The general circulation of the atmosphere is represented by ECHAM6.3 (Stevens et al., 2013) at a spectral horizontal resolution of T31 (about 3.75° on a regular grid) and with 31 vertical levels. At the surface, land processes including carbon and vegetation dynamics are simulated by JSBACH3.2 (Reick et al., 2013, 2021). Ocean dynamics are treated by MPIOM1.6 (Jungclaus et al., 2013) configured with a nominal horizontal resolution of 3° on an Arakawa C-grid (Arakawa and Lamb, 1977) with poles over Greenland and Antarctica, and 40 vertical levels. The ocean surface includes a zero-layer sea-ice thermodynamic module (Hibler, 1979). Carbon in the ocean is cycled by the biogeochemistry model HAMOCC6 (Paulsen et al., 2017; Ilyina et al., 2013). The coupled model setup includes adjustments in topography and land–sea mask once every decade as the reconstructed ice sheets change. These adjustments happen according to the bathymetry algorithm of Meccia and Mikolajewicz (2018), along with corresponding adaptation of runoff river routing on land as detailed in Riddick et al. (2018).

https://doi.org/10.5194/egusphere-2026-5687
Preprint. Discussion started: 2 November 2026
© Author(s) 2026. CC BY 4.0 License.

Table 1. Configuration of transient experiments of the last glacial cycle. The atmosphere and ocean components of the Earth system model were re-tuned in the ICE experiments of Mikolajewicz et al. (2025). An interactive module can be dynamic, disabled (off), or replaced by prescribed input data in the case of ice sheets and volcanoes. References for the data are in the main text.

			model parameters		*dynamic processes or prescribed data*				
Name	Age range	Reference	Atmosphere	Ocean	Land C	Ocean C	Methane	Ice sheets	Volcanoes
LGC	133–0 ka	this study	default	default	dynamic	off	dynamic	GLAC-1D	off
BGC	24–6 ka		default	default	dynamic	dynamic	dynamic	ICE-6G	off
ICE2.1	25–0 ka	Mikolajewicz et al.	re-tuned	re-tuned	dynamic	off	off	dynamic	PalVol
ICE2.2	25–0 ka	(2025)	default	re-tuned	dynamic	off	off	dynamic	PalVol

The standard model framework with prescribed ice sheets and carbon cycle has already been used in glacial–interglacial experiments (Kapsch et al., 2022; Duque-Villegas et al., 2025). Similarly, model variants with added complexity have run deglaciation experiments that consider: a dynamic methane (CH_4) cycle (Kleinen et al., 2020, 2023), dynamic ocean carbon cycle (Liu et al., 2024), land-to-ocean carbon transfers (Extier et al., 2022), and dynamic ice sheets, viscous solid-Earth and iceberg calving (Schannwell et al., 2024; Mikolajewicz et al., 2025). Overall, the model is suitable for such transient experiments and operates within uncertainty ranges of proxy data and other Earth-system models. In the following section we explain which configuration variants we use for experiments with different time scopes.

2.2 Experiments

We analyse a set of four MPI-ESM1.2 transient simulations summarized in Table 1. The experiments differ in complexity and run length, because each one incorporates a specific combination of interactive processes, to model carbon-cycle and ice-sheet dynamics, and modelling these interactively significantly increases the computational cost. Two of the experiments come from this study (LGC and BGC), while another two (ICE2.1 and ICE2.2) come from the previous work of Mikolajewicz et al. (2025). All the experiments have the same Earth orbital parameters calculated in agreement with Berger (1978), as well as the same prescribed levels of GHG radiative forcing of mixed CO_2, CH_4, and N_2O from the ice-core data synthesis by Köhler et al. (2017). This prescribed CO_2 series also drives plant photosynthesis, except in experiment BGC which uses interactive biogeochemistry. Atmospheric aerosols are kept constant at preindustrial levels (Kinne et al., 2013) and we assume no anthropogenic land use. Figure 1 shows important diagnostic variables from the prescribed forcings used in the simulations, albeit the ice-sheet variables apply only to experiments LGC and BGC.

LGC and BGC are transient experiments that we both run with prescribed ice sheets but different carbon cycle dynamics and time spans. LGC covers the entire last glacial cycle, spanning the last 133 kyr, with dynamic terrestrial carbon alone, while BGC is a much shorter experiment, covering only 18 kyr between roughly 24 ka and 6 ka. However, it includes an interactive marine carbon cycle that couples the full global carbon cycle and therefore simulates a prognostic atmospheric

https://doi.org/10.5194/egusphere-2026-5687
Preprint. Discussion started: 2 November 2026
© Author(s) 2026. CC BY 4.0 License.

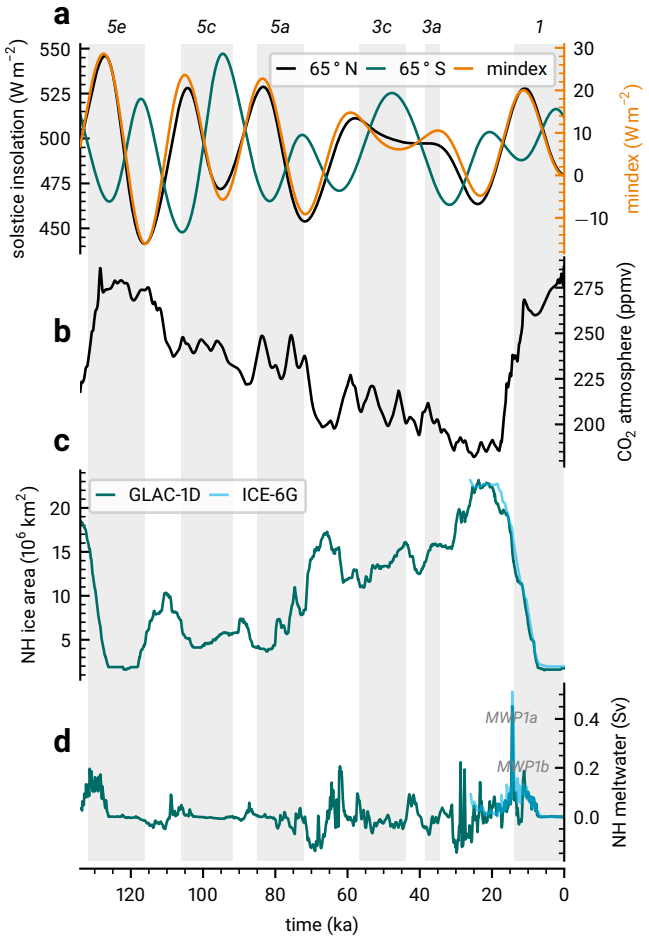


Figure 1. Last glacial cycle forcing in simulations: (a) solstice insolation of North and South latitude bands during their respective summer seasons, as well as the orbital monsoon index (mindex) of Rossignol-Strick (1983), according to the orbital parameters of Berger (1978); (b) atmospheric CO_2 from the ice-core data synthesis of Köhler et al. (2017); (c) Northern Hemisphere (NH) ice-cover area from reconstructions GLAC-1D and ICE-6G (references in main text); and (d) reconstructed estimated meltwater release from ice sheets, including annotations for meltwater pulses (MWP) 1a and 1b. Vertical shading highlights warm Marine Isotope Stages (MIS) by Railsback et al. (2015).

CO_2 concentration. Due to open questions in biogeochemistry modelling, we must nudge ocean alkalinity in experiment BGC, similar to the approach of Brovkin et al. (2019), to be able to approximately simulate CO_2 levels like those reconstructed from ice cores. Both experiments run with the dynamic methane cycle of Kleinen et al. (2020), which computes atmospheric levels of CH_4, although in this case it is only a diagnostic concentration and does not induce radiative forcing changes. Prescribed ice sheets in LGC follow the GLAC-1D reconstruction (Briggs et al., 2014; Tarasov et al., 2012), while in BGC we use the ICE-6G reconstruction (Peltier et al., 2015). Hence, differences in topography and meltwater history between ice-sheet reconstructions also affect experiment comparisons (e.g. Kapsch et al., 2022).

https://doi.org/10.5194/egusphere-2026-5687
Preprint. Discussion started: 2 November 2026
© Author(s) 2026. CC BY 4.0 License.

We include in our analyses also the experiments D2.1 and D2.2 from Mikolajewicz et al. (2025), which for clarity in our case appear labelled as ICE2.1 and ICE2.2. The main reason to complement our experiments with these other two is that in previous work we noticed a lack of millennial-scale variability in our runs with prescribed ice-sheets (Duque-Villegas et al., 2025). Because ice-sheet and solid-Earth dynamics, as well as iceberg calving, were interactive in these ICE experiments, Heinrich-like cooling events could emerge unforced in the simulation, providing insight into rapid climate responses. Furthermore, Mikolajewicz et al. (2025) re-tuned some model parameters in these experiments, due to poorly constrained processes like ocean background mixing and atmospheric cloud properties. Including both experiments therefore broadens our simulation variability range and provides a more robust basis for identifying features that consistently emerge across experiments. Unlike LGC or BGC, these ICE experiments included an additional forcing factor in the form of stochastic volcanic variability from the PalVol v1 reconstruction (Schindlbeck-Belo et al., 2024). Further important differences explain why we expect ICE experiments to have less extra-tropical tree cover than the LGC or BGC ones: first, the ICE experiments had a slightly higher energy threshold for extra-tropical tree growth (known as the minimum of growing degree days or GDD), and second, the ICE experiments had stronger wind damage effects (wind-break and wind-throw).

3 Results

For all experiments we produce global data sets averaged at a centennial resolution and in the analyses we ignore the first 1 kyr of each simulation to avoid the effects of initialization adjustments. The results focus on the evolution of terrestrial vegetation and the global carbon cycle. For deviations relative to a preindustrial state (PI) we use the time average of 1 ka to 0 ka (1 kyr) of a simulation as a reference. We start by evaluating simulated trends in large-scale mean values and afterwards we study how vegetation changes translate into terrestrial emissions of GHG.

3.1 Global and hemispheric trends

At the start of the LGC simulation, near the Last Interglacial (Eemian) around 125 ka, the planet warms very slightly (+0.5 K) above preindustrial levels (Fig. 2a), briefly for a few centuries, and thereafter a prolonged cooling trend evolves until reaching a global minimum near the LGM at about 24 ka, that is some 5 K colder than the preindustrial era. This is a slightly smaller change than the estimates of almost 6 K of Tierney et al. (2020) or 7 K of Osman et al. (2021). After this, the planet warms again into the Holocene. The BGC and ICE experiments follow LGC in the warming trend out of the LGM, yet BGC evolves slightly warmer into the Holocene. In comparison with the temperature reconstruction of Snyder (2016), the simulations underestimate deviations from PI. Nevertheless, the simulations stay close to uncertainty intervals and evolve rather similarly as the reconstruction.

Superimposed on the global temperature trends there are some brief cooling excursions, related to severe weakenings of the Atlantic meridional overturning circulation (AMOC), from its maximum strength at 26.5° N below 400 m depth (Fig. 2b). It weakens most markedly before the Holocene onset, near the early boundary of Marine Isotope Stage (MIS) 1. The experiments LGC and BGC have a near-complete shutdown of AMOC around the strong Meltwater Pulse 1a (MWP-1a) near 14.5 ka,

https://doi.org/10.5194/egusphere-2026-5687
Preprint. Discussion started: 2 November 2026
© Author(s) 2026. CC BY 4.0 License.

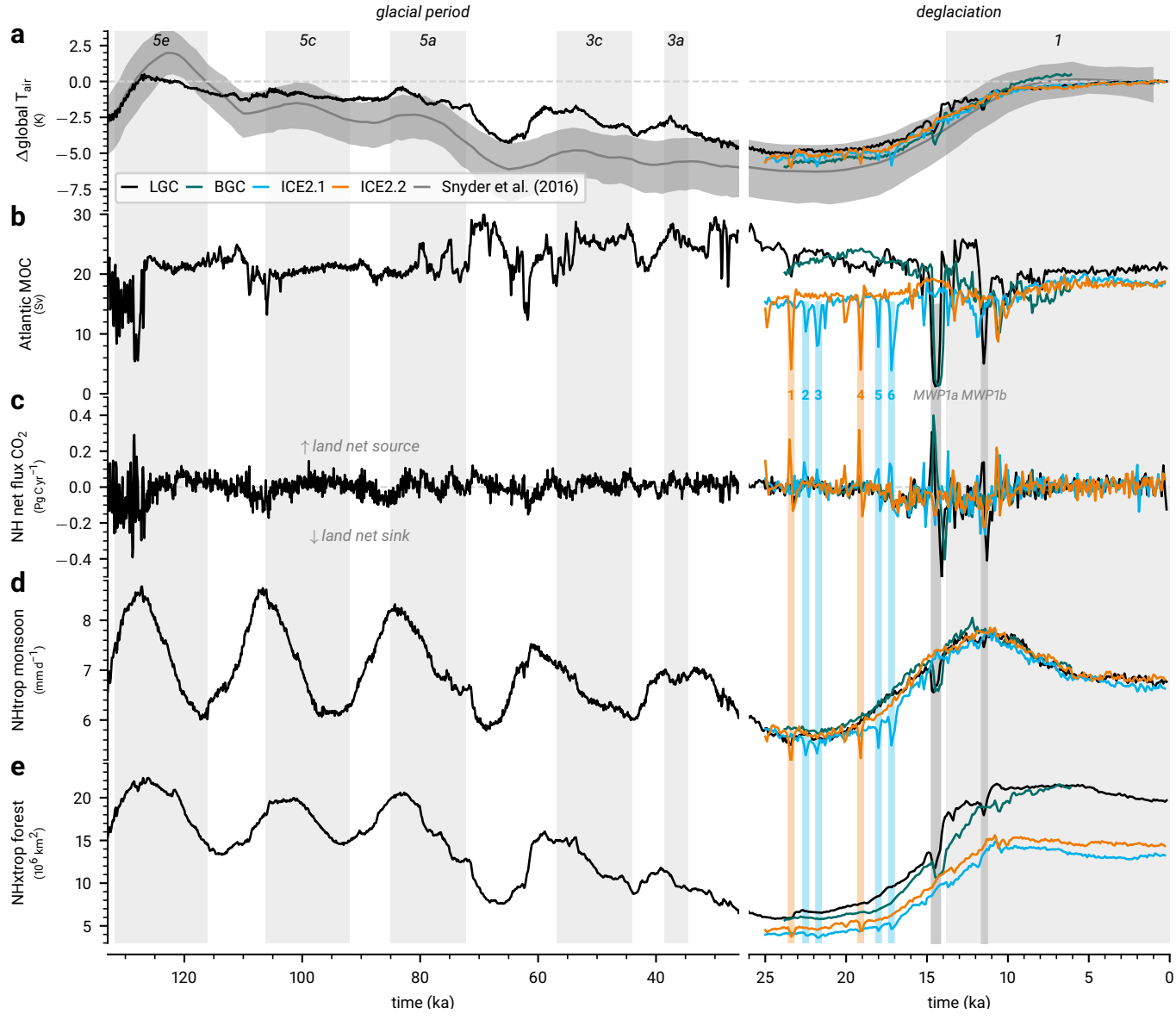


Figure 2. Simulated climate globally: (a) change from preindustrial mean near-surface temperature (T_{air}) compared with the reconstruction by Snyder (2016); (b) maximum Atlantic meridional overturning circulation (MOC) near 26.5° N and below 400 m depth; (c) Northern Hemisphere (NH) net CO_2 flux from land into the atmosphere; (d) continental rainfall within the monsoon region calculated like Liu et al. (2009) in the NH tropics (NHtrop) from 0° to 30° N; and (e) forest cover in the NH extra-tropics (NHxtrop) from 30° N to 90° N. The horizontal time axes separate the last glacial period and deglaciation. Vertical light shading shows isotopic stages like in Fig. 1, while dark and coloured vertical shading in (b) to (e) highlights labelled cooling events in the North Atlantic.

https://doi.org/10.5194/egusphere-2026-5687
Preprint. Discussion started: 2 November 2026
© Author(s) 2026. CC BY 4.0 License.

synchronous with a global cooling of about 1 K. Such variability agrees with previous simulations in Kapsch et al. (2022). LGC additionally shows substantial AMOC weakening during Meltwater Pulse 1b (MWP-1b) near 11.5 ka. The experiments ICE2.1 and ICE2.2, having a differently tuned ocean mixing and dynamic ice sheets, result with a weaker AMOC than LGC or BGC, and they lack the severe MWP changes. Instead, ICE2.1 and ICE2.2 exhibit repeated weakening spikes related to Heinrich-like surge events (Mikolajewicz et al., 2025). In Fig. 2b we label these quick AMOC excursions sequentially, and note that the strongest AMOC weakening happens at spikes 1, 4, and 6, almost matching the MWP-1a change, though only briefly.

Temperature and AMOC variations have a clear impact on the net balance of terrestrial carbon (Fig 2c). In all simulations, the time-averaged net CO_2 flux from NH land fluctuates closely around zero net exchange, except when strong AMOC disturbances occur. Soon after the AMOC weakens, the NH land turns into a net carbon source of somewhere between nearly $0.15\,\mathrm{Pg\,C\,yr^{-1}}$ to over $0.40\,\mathrm{Pg\,C\,yr^{-1}}$, depending on the experiment and AMOC disturbance. However, as Atlantic circulation is restored, NH land switches into a carbon sink of similar magnitude. Experiment ICE2.2 shows strong source spikes at events 1 and 4, but the subsequent sink response is much more muted. How much carbon remains in the atmosphere depends on the duration of source and sink periods; we look more closely at the land interaction with the atmospheric and oceanic carbon cycles when we focus on experiment BGC in Section 3.4.

The relationship between AMOC variability and the carbon cycle is complex, but we initially focus on moisture changes and consider what happens to rainfall within the tropical monsoon domain in the NH (Fig. 2d). We estimate the monsoon domain according to Liu et al. (2009). The hemispheric monsoon moisture trend in experiment LGC shows quasi-periodic variations with peak levels at the start of warm MIS stages, resembling orbital cycles (see Fig. 1a), and it becomes drier as it approaches the LGM. Such slow cycles also appear in moisture-related proxy data from Brazil (Cruz et al., 2005) and Asia (Cheng et al., 2016). Yet if we look closely at experiments ICE2.1 and ICE2.2 during the early part of the deglaciation, we see that the faster AMOC variability spikes are also superimposed over the monsoon rainfall trend. Experiments LGC and BGC also display a weakening AMOC effect on tropical moisture during MWPs before the Holocene onset, because of the severe disturbance to ocean circulation. That a weaker AMOC modifies the meridional Atlantic sea-surface temperature (SST) gradient and leads to a displacement of tropical rain bands has been found in geological records and simulations (Lawman et al., 2025).

Beyond the tropics in the NH, vegetation on land also changes slightly in connection with AMOC variability (Fig. 2e). In the LGC experiment, the trend of forest cover extent in the northern extra-tropics fluctuates with precessional pace around almost $20 \times 10^6\,\mathrm{km^2}$. There is a minimum forest extent of about $6 \times 10^6\,\mathrm{km^2}$ at the LGM. Unlike experiments LGC and BGC, the ICE2.1 and ICE2.2 experiments have substantially less forest cover in this region, not only because of the different GDD parameter for extra-tropical trees, but also because these experiments simulate stronger wind damage (see end of Section 2.2). Despite having less forest, experiments ICE2.1 and ICE2.2 still show small kinks in forest cover tracking the Heinrich-like events. A much larger change in forest cover occurs in LGC and BGC during MWP-1a, when almost $2 \times 10^6\,\mathrm{km^2}$ are quickly lost and soon afterwards recovered, with a sharp rise in forest cover as both experiments transition into MIS 1.

https://doi.org/10.5194/egusphere-2026-5687
Preprint. Discussion started: 2 November 2026
© Author(s) 2026. CC BY 4.0 License.

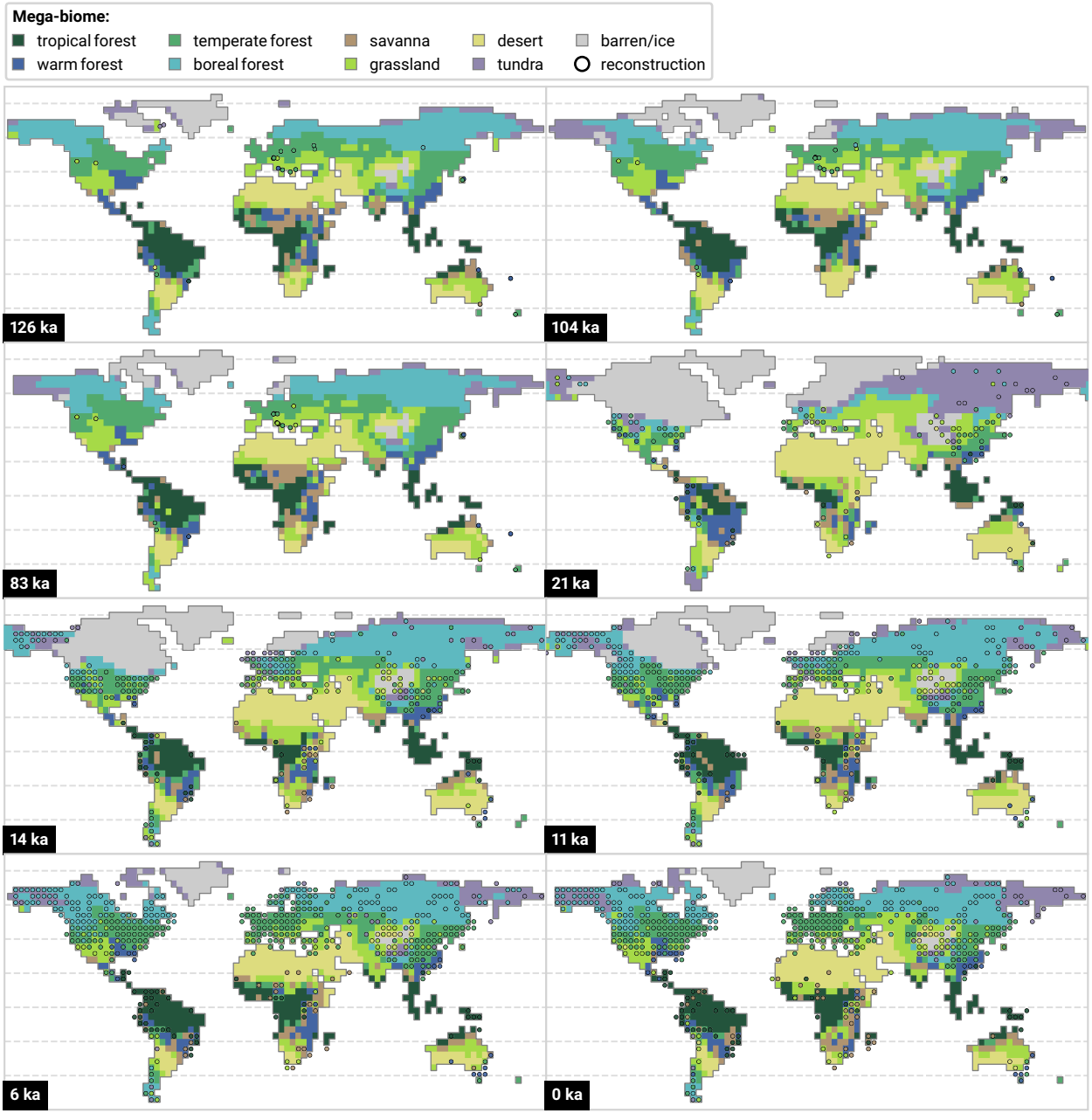


Figure 3. Biomes of simulated vegetation cover fractions in the LGC experiment, according to the method of Dallmeyer et al. (2019), for: peak warm MIS 5 stages (at 126, 104, and 83 ka); near the LGM (at 21 ka); the Bølling–Allerød (near 14 ka); the early (around 11 ka) and middle (at 6 ka) Holocene; and PI state (at 0 ka). Reconstructed biomes from pollen data (filled circles) are taken from Hoogakker et al. (2016) and Li et al. (2025) as explained in the main text. See the online version for a close comparison with pollen data.

https://doi.org/10.5194/egusphere-2026-5687
Preprint. Discussion started: 2 November 2026
© Author(s) 2026. CC BY 4.0 License.

3.2 Vegetation of the last glacial cycle

Simulated climate results in the vegetation patterns shown as mega-biomes for selected intervals in Fig. 3. Biome groups are useful in this case to summarize in a single map the simulated cover fractions of multiple plant functional types (PFTs) at each grid point, while taking into account bioclimatic limits according to the simulated climate (Dallmeyer et al., 2019). For a qualitative comparison, we also overlay available pollen-based reconstructions: from Hoogakker et al. (2016) for times before the LGM (using a 7-kyr search width because of temporal resolution differences) and from Li et al. (2025) for times between LGM and the preindustrial era. The reconstruction of Li et al. (2025) aligns perfectly with our model grid because they included the model we use in their methods.

Considering that both field evidence and reconstructions are clustered in North America, Europe and eastern Asia, and that most reconstructions that exist reach only as far back as the LGM, we nevertheless find a reasonable overall representation of shifting vegetation during the full glacial cycle. Some notable discrepancies occur in Beringia, where the model favours tundra cover rather than the boreal biome, and in Europe near the Bølling–Allerød (BA) warming around 14 ka, where the opposite occurs with the model simulating forest cover where reconstructions show tundra. Also in northern Africa, although Saharan greening is simulated, it is weak compared with pollen-based reconstructions which suggest forest cover where the model simulates grass cover. Yet the simulation agrees with reconstructions about the position of the boreal treeline in Eurasia around the mid-Holocene (6 ka), as well as about an east-west partition of temperate versus boreal forest biomes in North America.

The most striking land-cover changes during the entire glacial cycle are, firstly, the boreal forest replacement by tundra in eastern Eurasia as the planet cools approaching the LGM (compare 126 ka and 21 ka in Fig. 3), and secondly, the northward extension of savanna and forest cover during episodes of Saharan greening in northern Africa (compare any of 126, 104, 83, and 6 ka with 0 ka). It is also interesting to see the encroachment of a narrow ice-free corridor in North America during the early Holocene near 11 ka by boreal tree cover, because it demonstrates the speed of vegetation spreading into ice-free land in the model (this also happens in the BGC, ICE2.1 and ICE2.2 experiments; not shown). In the inner tropics (south of 5 °N) the largest changes also include the break-up of the tropical forest biome in the Amazon, as the planet approaches the LGM. Only a core northwest-southeast transect remains always as tropical forest biome in the Amazon.

Biomes in Fig. 3 are in broad agreement with the BIOME4 estimates by Hoogakker et al. (2016) and the LPJ-GUESS estimates by Allen et al. (2020). Despite differences in spatial resolutions and ice-sheet reconstructions, the patterns usually place similar biomes around similar locations within close time intervals. Some notable differences are, first, that our experiment LGC simulates larger subtropical deserts in the Southern Hemisphere (SH), and second, that biome patterns from LGC have a more zonal west–east structure. Hoogakker et al. (2016) also consistently show a greater extent of grasslands across the NH, in places where our LGC simulation shows forest cover, like in northern Africa and the high latitudes.

https://doi.org/10.5194/egusphere-2026-5687
Preprint. Discussion started: 2 November 2026
© Author(s) 2026. CC BY 4.0 License.

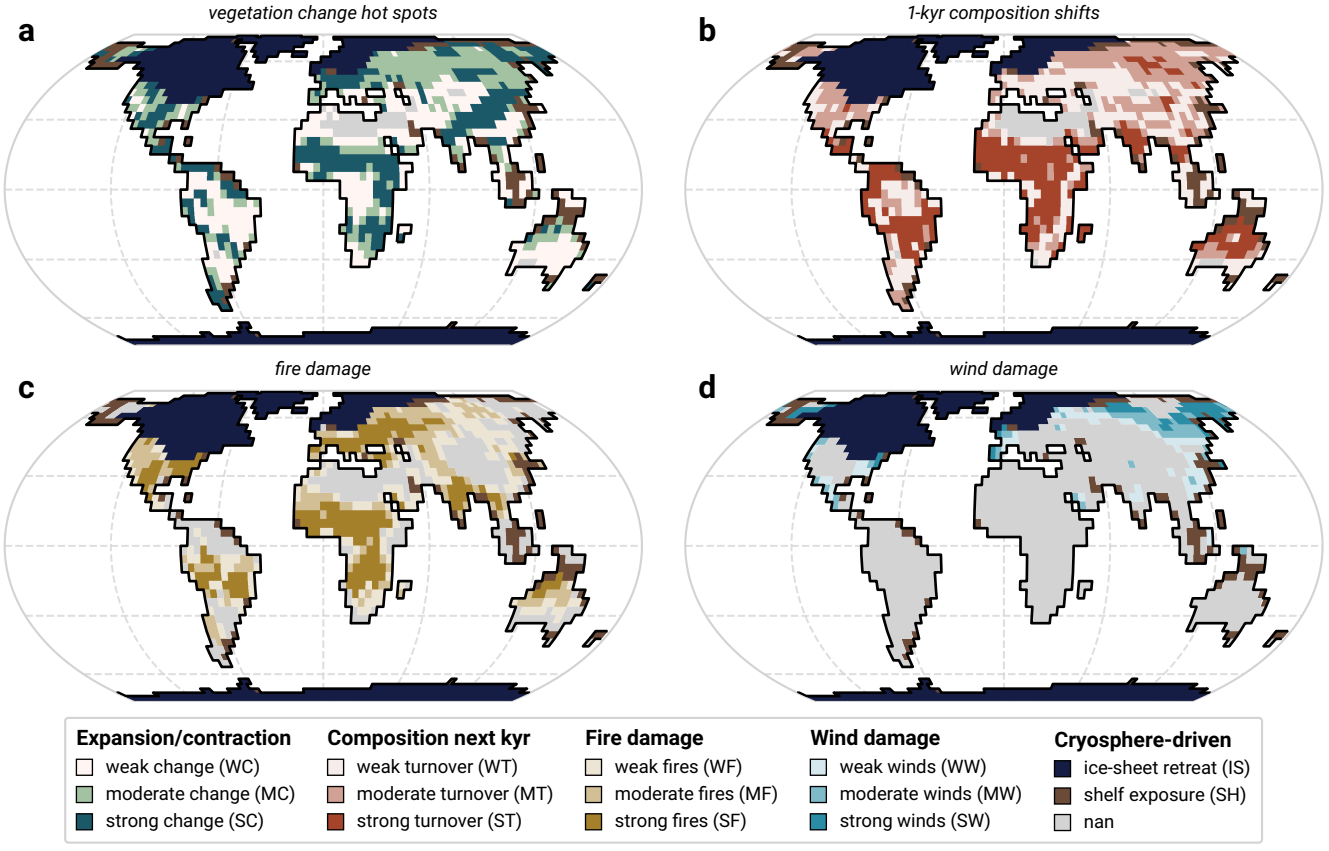


Figure 4. Types of vegetation change in experiment LGC: (a) highly dynamic vegetation zones; (b) maximum potential for PFT composition shifts within a 1 kyr interval; (c) fire damage hot spots; and (d) wind damage of woody types. All panels have cryosphere-driven regions with ice sheets (IS) and shelf exposure (SH) masked out (nan). Regions where total vegetation cover is always below 10 %, or where maximum disturbance damage affects are less than 1 km^2 are also masked out. The weak (W), moderate (M), and strong (S) classification is based on terciles (cutoff points at $1/3$ and $2/3$ percentiles) of the standard deviation of the respective land variables. Parentheses show labels for each coloured region. Compositional change is based on the maximum squared-chord distance of all PFT fractions at 1-kyr steps.

3.3 Classification of vegetation change

The reconstruction of biomes helps us to broadly assess model performance. However, the distinction between vegetation classes and geographic ranges is not as relevant for the global carbon cycle as the patterns of change that reflect land transformations capturing or releasing carbon in exchange with the atmosphere. Figure 4 separates types of vegetation changes that, by varying degrees, affect the global carbon cycle in experiment LGC. We first mask out the regions where the vegetation response during the glacial cycle is strongly affected by the ice-sheet reconstruction, as well as by its concomitant sea level adjustment (continental shelf areas). Next, we classify variability changes based on terciles of the standard deviation of the entire glacial cycle for specific land surface variables: “weak” (W) is below a one-third cutoff in variation, while “strong” (S) is above the

https://doi.org/10.5194/egusphere-2026-5687
Preprint. Discussion started: 2 November 2026
© Author(s) 2026. CC BY 4.0 License.

two-thirds mark in variation, and what is left in between are "moderate" (M) changes. We also use absolute magnitude values to mask out places where total vegetation is never above $10\,\%$ cover, and where the maximum disturbance damage affects an area smaller than $1\,\mathrm{km}^2$. We define specific region labels based on keywords and the tercile initials: change (WC, MC, and SC), turnover (WT, MT, and ST), fire (WF, MF, and SF), and wind (WW, MW, and SW).

Vegetation change hot spots are found by analysing changes in total vegetation cover at each location, and they highlight regions with pronounced growth or die-back phases, as well as transition areas with shifting vegetation boundaries (Fig. 4a). Compositional changes are detected from the simultaneous analysis of the multiple PFT cover fractions (Fig. 4b), by calculating the square-chord distance (SCD) between consecutive time steps at 1-kyr spacing (e.g. Overpeck et al., 1985). SCD is an index that is bound between 0 (identical composition across 8 PFTs) and 2 (completely different compositions). In this case we compute the time-maximum possible compositional change and classify the changes using again tercile cutoff values of $2/3$ and $4/3$ (because of the 0 to 2 range of the index).

As expected, the regions with the largest changes are generally transition areas that surround densely vegetated centres, like in the tropics and eastern Asia (Fig. 4a). These transitional areas have a vegetation-growth front that expands northward across northern Africa and south-eastern Asia. Both are regions where monsoon rainfall is enhanced during globally warm periods (see Fig. 2d). Much of Europe, sitting downwind from the Laurentide ice sheet and close to the Fennoscandian ice sheet, also has a strong variability in vegetation cover. Similarly, there is strong variability following the northern Atlantic coastline of South America into Central America. Conversely, over much of the Amazon, central Africa, the Afro-Asian desert corridor, eastern Asia, the Maritime Continent, and Australia, total vegetation changes only weakly across the entire glacial cycle.

However, regions with little change in total coverage can still experience compositional shifts in PFT fractions at scales relevant for the global carbon cycle. Here we focus on maximum possible composition turnover after one millennium. For instance, Fig. 4b shows an arc of moderate turnover in eastern Siberia, where there is taiga-to-tundra replacement; also visible in Fig. 3. We detect a strong, ring-like, composition shift in the Amazon, at the edges where tropical forests can be replaced by savanna or warm temperate mixed biomes. In northern Africa, the concentrated turnover region matches the highly dynamic vegetation change hot spots, as expected when close to nil PFT fractions are replaced with at least some vegetation cover.

Shifting vegetation margins and composition re-shuffling in the LGC experiment are mainly related to $\mathrm{CO_2}$ and climate-driven adjustments in net-primary productivity (NPP) and PFT-competition that modify growth rates around the globe. As a reference, experiment LGC simulates a drop in global NPP from the preindustrial reference by about $50\,\%$ near the LGM (from $62.2\,\mathrm{Pg\,C\,yr^{-1}}$ to $31.3\,\mathrm{Pg\,C\,yr^{-1}}$). In addition, vegetation dynamics in the simulation also depend on disturbances that vacate land fractions for new PFT growth. In the model there is damage by fire equally for all PFTs, or wind-break and wind-throw damages only on woody plant types. Figure 4c shows that the largest fire-induced changes happen around the tropics, especially in Africa and India, whereas the largest wind-induced damages occur in northeastern Eurasia, as well as on both North American and European coasts on the Atlantic (Fig. 4d). Although fire and wind disturbances have a comparatively smaller impact on the natural land cover than climate or productivity changes, they complete the set of forces acting on vegetation cover and help understand the patterns in Figs. 4a and b.

https://doi.org/10.5194/egusphere-2026-5687
Preprint. Discussion started: 2 November 2026
© Author(s) 2026. CC BY 4.0 License.

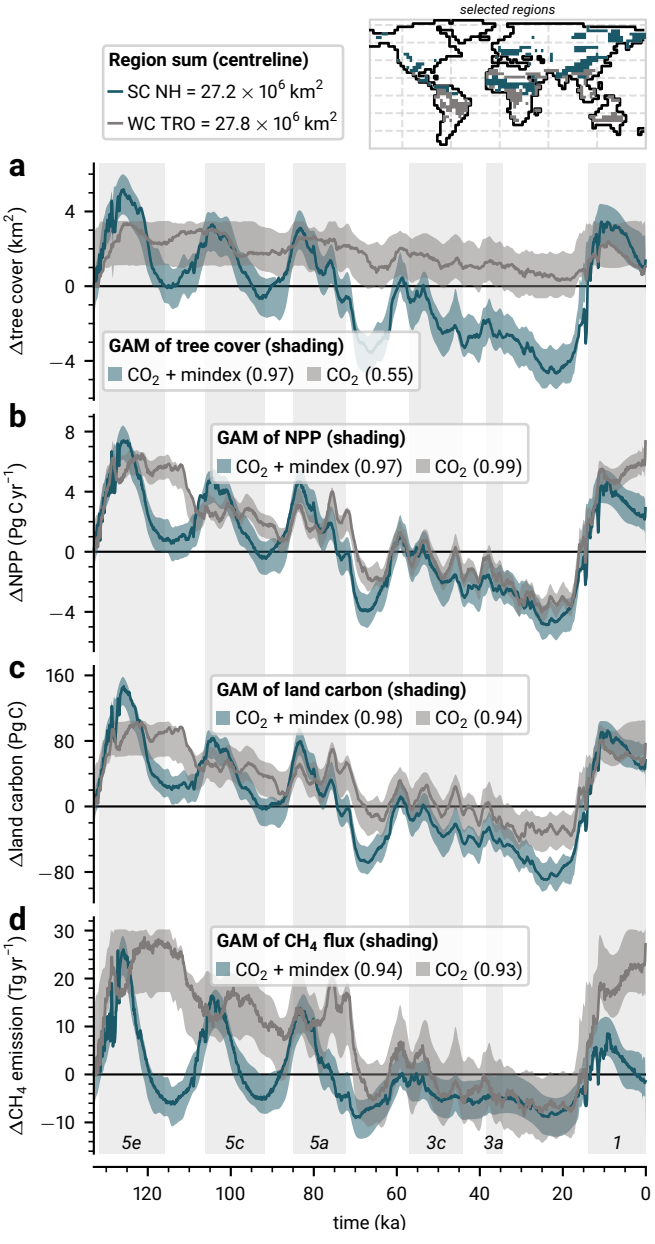


Figure 5. Changes in regional totals from experiment LGC as predicted by atmospheric CO_2 and a lagged orbital monsoon index (mindex) after fitting generalized additive models (GAMs) of: (a) tree cover extent; (b) net primary productivity (NPP); (c) land carbon storage; and (d) net methane emissions. The orbital predictor is lagged by 1.5 kyr. Regions SC and WC are the same from Fig. 4a, but narrowed down here to only the NH (SC NH: 0–90° N), or the tropics (WC TRO: 30° S–30° N). Centrelines (solid lines) are the simulated values from the LGC experiment, while enclosing shading shows GAMs prediction intervals. Parentheses show the adjusted R^2 of each fit.

https://doi.org/10.5194/egusphere-2026-5687
Preprint. Discussion started: 2 November 2026
© Author(s) 2026. CC BY 4.0 License.

3.4 Terrestrial carbon at orbital scale

Patterns of vegetation cover change and disturbance activity also define the terrestrial storage of carbon and its exchange with the atmosphere. They reflect a redistribution of standing biomass, litter production, and carbon accumulation in the soils, while changing environmental conditions alter the balance between NPP (atmospheric carbon sink) and soil respiration (atmospheric carbon source). Fires result in direct CO_2 emissions, while wind damage moves carbon into the soil carbon pools, where it turns into CH_4 emissions under anaerobic conditions (inundated areas in the model). Changes in these natural emission pathways are summarized in Fig. 5 for the LGC experiment in two hemispheric regions with distinct vegetation dynamics: the strongly variable parts of the NH (SC NH) versus the weakly changing parts within the tropics (WC TRO), as defined in Fig. 4a. Even though these regions cover vastly different territories, they both amount to areas slightly larger than $27 \times 10^6\,\mathrm{km}^2$.

Over these two regions, the simulated changes in tree cover (Fig. 5a), land NPP (Fig. 5b), land carbon (Fig. 5c), and net methane emissions (Fig. 5d) all show two different modes of variation: one sinusoidal pattern with positive phases during warm intervals (e.g. MIS 5e, 5c, 5a, and 1), versus a long-term decline pattern with a sharp rebound after the LGM. Such temporal patterns resemble the contrast between the time series of a periodic orbital forcing (Fig. 1a) and a trend-driven CO_2 curve (Fig. 1b). In fact, we are able to skilfully predict these variations using the forcing data as predictors of generalized additive models (GAMs; Simpson, 2018). In the models we use ten cubic splines and as predictors we have either CO_2 alone or together with the orbital monsoon index (mindex). In this case we lag the orbital monsoon index by some $1.5\,\mathrm{kyr}$ to improve the GAM fits slightly, because this index is a boreal summer metric, while the vegetation cover peak is also a function of having tolerably cold winters, which are in anti-phase with peak summer insolation. In Fig. 5 the GAMs are shown according to their prediction intervals (at $95\,\%$ level) and we report the adjusted R^2 values as goodness-of-fit scores that measure explained variance.

Only for the changes in tree cover in the tropical WC TRO region there is a poor GAM fit using CO_2 alone as a predictor. For the rest of the variables the GAMs reproduce the regional variations rather well. Although it is possible that more complicated fitting techniques or other additional sets of predictors improve the GAM skill in each case, we find that this approach already shows that global trends at orbital scale in the carbon cycle can be represented as simple functions of such known forcing variables. While land carbon in parts of the NH (e.g. Sahara) changes strongly according to orbital precession and CO_2 levels, in other regions such as within the tropics, where vegetation cover stays high and fairly constant, land carbon changes mainly according to CO_2 alone.

3.5 Marine carbon contribution

Net natural carbon emissions from land are often counterbalanced by ocean regions that capture CO_2. Such ocean regions also changed physically and biochemically during glacial cycles, making it difficult to predict (i.e. model) when carbon stays airborne and for how long. In experiment BGC we investigate the interaction between land and ocean branches of the global carbon cycle during the interval from the LGM till the mid-Holocene (Fig. 6). Because there are still open questions about the deglaciation carbon budget, we resort to alkalinity nudging in this experiment to reproduce a realistic evolution of simulated atmospheric levels of CO_2 (e.g. Brovkin et al., 2019). Without alkalinity nudging the model can simulate only a fraction of

https://doi.org/10.5194/egusphere-2026-5687
Preprint. Discussion started: 2 November 2026
© Author(s) 2026. CC BY 4.0 License.

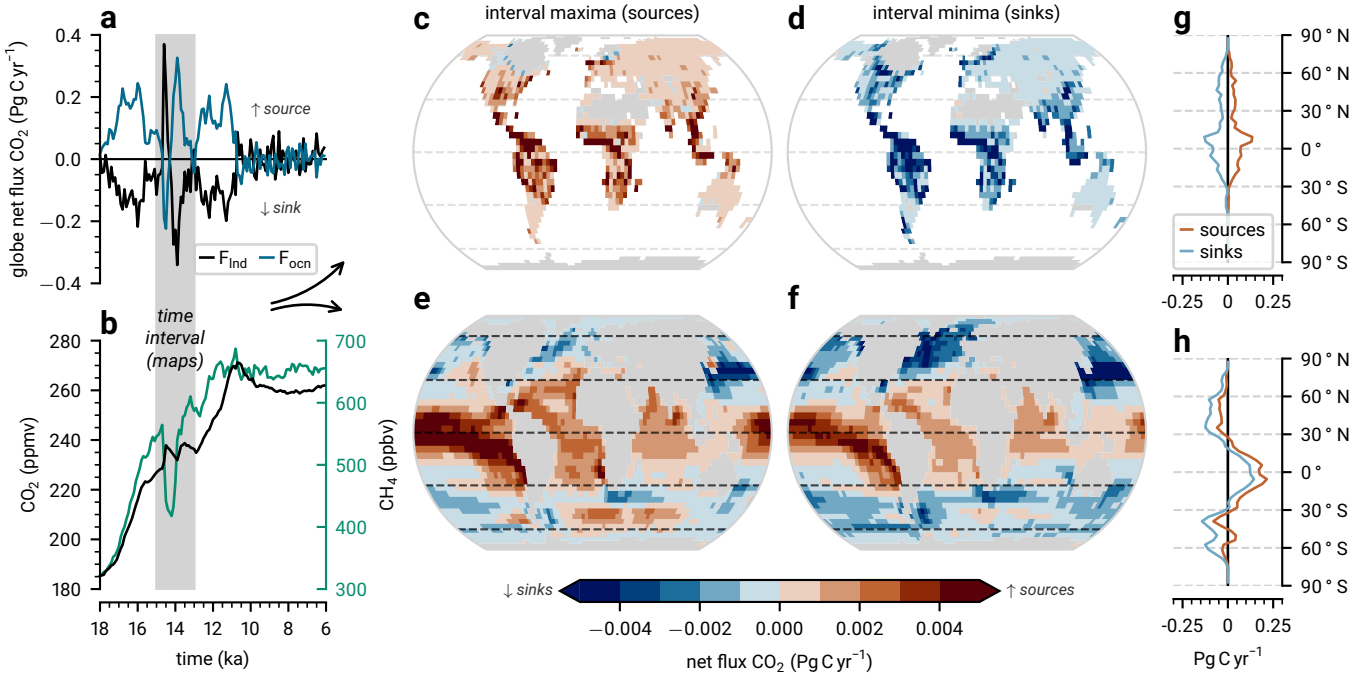


Figure 6. Ocean contribution to deglaciation carbon emissions in experiment BGC: (a) net flux of CO_2 from land (F_{lnd}) and ocean (F_{ocn}) to atmosphere; (b) simulated atmospheric levels of CO_2 and CH_4; (c) land and (d) ocean maximum potential for CO_2 emissions (source potential) within time interval around MWP-1a (gray in a and b), as well as (e) and (f) respectively, but for minimum potential (or sink potential); and (g) and (h) are zonal sums of potential land or ocean sources and sinks.

the roughly 90 ppmv deglacial rise in CO_2, and although our results could still show similar trends as in experiment BGC, all carbon fluxes and vegetation changes would be much more subtle.

In our model simulations as the planet warms out of the LGM, terrestrial productivity increases and the land is a net carbon sink (taking up some 0.2 $\mathrm{Pg\,C\,yr^{-1}}$), which lowers atmospheric partial pressure of CO_2 and the ocean becomes a net carbon source (Fig. 6a). These trends last until MWP-1a near 14 ka, when the sudden AMOC weakening turns the land briefly into a net source of carbon of almost 0.4 $\mathrm{Pg\,C\,yr^{-1}}$. Some of this carbon, however, is simultaneously compensated for by equally briefly ocean capture due to a much colder North Atlantic (about 0.2 $\mathrm{Pg\,C\,yr^{-1}}$ uptake). Because not all carbon is captured by the ocean, we see a sudden rise in atmospheric levels of CO_2 (Fig. 6b). Conversely, during this time methane levels drop sharply. Following MWP-1a, terrestrial ecosystems recover their post-glacial productivity and return to acting as a net carbon sink, with high carbon uptake rates persisting for several centuries and drawing atmospheric CO_2 down. In sum, for atmospheric CO_2 this MWP-1a disturbance results in a sudden rise by almost 10 ppmv, followed by a quick drop of about 6 ppmv, all within a few centuries. Methane has a more drastic oscillation of about 150 ppbv. After the simulation arrives at the Holocene, the balance between land and ocean fluxes is restored, leaving approximately 260 ppmv of CO_2 in the atmosphere by the end of the experiment (as expected according to the nudging and Fig. 1b).

https://doi.org/10.5194/egusphere-2026-5687
Preprint. Discussion started: 2 November 2026
© Author(s) 2026. CC BY 4.0 License.

The spatial patterns of these carbon transfers are difficult to analyze because sources and sinks are often changing. In Fig. 6c to 6f we focus on a time interval around MWP-1a, and separate the extreme values of land and ocean contributions, which are also zonally aggregated in panels Fig. 6g and 6h. The strongest potential for land carbon sources occurs within the tropics, inside the 0° to 30° N band (Fig. 6g), with a clear peak at 9° N. This peak coincides with the location of a precipitation maximum, linked to the Intertropical Convergence Zone (ITCZ) position during boreal summer, calculated according to Adam et al. (2016), which suddenly shifts southward by almost 1° during this time (see Fig. S4 in supplement). The subsequent recapture of carbon by the land sink appears symmetrically opposed to the sources, although it is worth remembering that timing at each grid point may differ within this interval. The symmetry means that the same vegetation cover that is lost, grows again after the disturbance. In the ocean a general structure is maintained, with the tropics always being a net source of carbon and the extra-tropics almost always being a net sink (Fig. 6h). However, in Fig. 6f we see what happens when the AMOC is weaker, which is when the colder NH ocean becomes a larger net sink, while in Fig. 6d we see how the Southern Ocean south of Africa becomes a net source at some point within the time interval around MWP-1a.

3.6 Fast carbon transfer rates

The strong response of vegetation cover to large and sudden meltwater pulses constitutes a fast interaction timescale in the global glacial–interglacial carbon cycle that requires only a few centuries. The coupling mechanism has the largest consequences for the NH tropics (Fig. 6g), where net emissions of CO_2 during MWP-1a represent about 70 % of the global emissions (Fig. 7a). In experiment BGC, for instance, this amounts to a woody cover loss of almost $4 \times 10^6\,\mathrm{km}^2$ within six centuries, together with a loss of herbaceous types close to $1 \times 10^6\,\mathrm{km}^2$. Beyond MWP-1a, the simulation LGC also shows fast CO_2 outbursts before the Eemian interglacial (Fig. 7a), in response to meltwater disturbances, as the ice sheets from the penultimate glaciation break up, and again before the start of warm MIS 5c stage (see meltwater in Fig. 1d). Experiments ICE2.1 and ICE2.2 also have repeated CO_2 outbursts corresponding with all of the numbered Heinrich-like events, except event 3, although some of these have only about half the magnitude of the others (from LGC and BGC) during MWP-1a. Heinrich-like event number 3 probably happened too closely after event number 2 for vegetation to have been completely restored. While comparing these outbursts between LGC, BGC and the ICE experiments it becomes important to remember that ICE experiments have overall less forest cover, which also limits the magnitude of these outbursts.

Methane emissions from the tropical NH resemble the pattern in Fig. 5d, bearing the orbital precession signal. However, when we take the time (first-finite) derivative of these emissions (Fig. 7b), we can identify sudden changes in the rate of emissions that we consider methane "outbursts" when positive, or "slowdowns" when negative. These events tend to happen during cold isotopic stages, preceding the beginning of warm phases, yet this is not always the case, and the correspondence with CO_2 fluxes is weak outside of the strong meltwater events before the Eemian and Holocene interglacials. Besides soil carbon, methane production (and subsequent release) also depends on temperature and moisture, therefore sudden changes require a strong enough disturbance to make all three variables respond quickly. ICE experiments did not include the dynamic methane component, so their Heinrich-like events do not appear in the methane analysis.

https://doi.org/10.5194/egusphere-2026-5687
Preprint. Discussion started: 2 November 2026
© Author(s) 2026. CC BY 4.0 License.

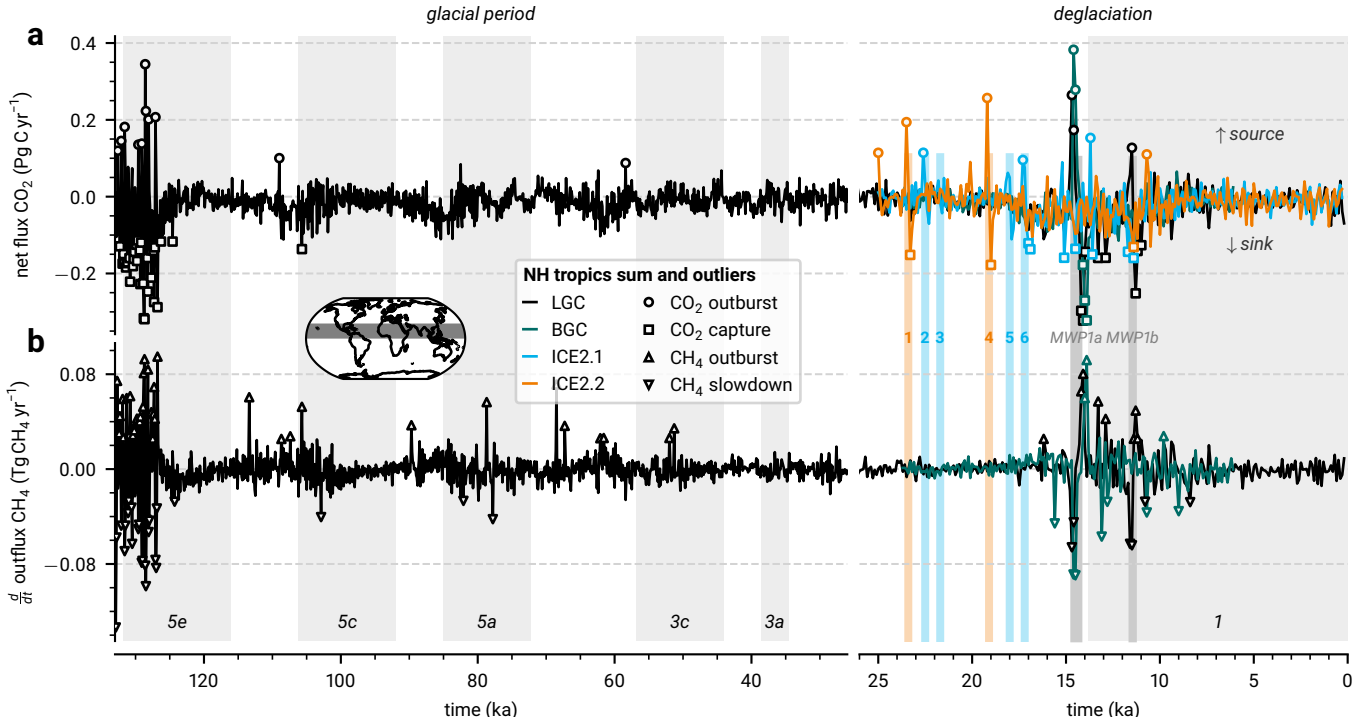


Figure 7. Fast carbon transfers from land GHG emissions within the tropical NH (0° to 30° N) from (a) the net flux of CO_2 in all experiments, as well as (b) the time derivative of the net CH_4 emissions only in experiments LGC and BGC. Outliers are detected using z-scores of the median of absolute deviations from the median and a cutoff value of 4. Besides the vertical bars of isotopic stages like in Fig. 2, there is dark and coloured vertical shading representing events of strong cooling of the North Atlantic.

4 Discussion

Experiments LGC, BGC, ICE2.1, and ICE2.2 together capture the salient dynamics of the last glacial–interglacial cycle: orbitally induced variations in insolation, changing atmospheric CO_2 levels, biome shifts, methane from wetlands, abrupt cryosphere–ocean interactions, and marine carbon exchange with the atmosphere. We have simulated the trajectories of the global carbon and methane budgets, featuring distinct timescales of change depending on specific drivers which are especially relevant for low-latitude regions without ice-sheet growth. First, a productivity fluctuation tracking CO_2 with little cover change (Fig. 5), second, a precession-paced redistribution of terrestrial carbon stocks and methane emissions (Fig. 5), and third a meltwater-controlled abrupt release of tropical carbon (Fig. 7). These interactions relate to the different response times of vegetation cover to environmental change, according to effects on productivity, cover types competition, bioclimatic limits, or disturbances, which combine to produce biome shifts and variable GHG emissions.

https://doi.org/10.5194/egusphere-2026-5687
Preprint. Discussion started: 2 November 2026
© Author(s) 2026. CC BY 4.0 License.

4.1 Natural CO_2 fertilization of quasi-static biomes

That elevated levels of atmospheric CO_2 enhance net carbon fixation via photosynthesis is an effect known in the context of rising anthropogenic emissions as "CO_2 fertilization" (Ainsworth and Long, 2005). Even though plant responses to CO_2 changes are complex (Körner, 2006) and in spite of atmospheric CO_2 being almost always below preindustrial levels in our experiments (Fig. 1b), we also use this term to refer to the ecophysiological effects of CO_2 on net vegetation productivity (Gerhart and Ward, 2010). Claussen et al. (2013) found that in a previous version of the model we use such effects alone explain most of the glacial "thinning" of vegetation at the LGM, with a secondary contribution by the thermodynamic effects of lower CO_2 levels. The reduction in LGM productivity by about 50 % in our experiments is well aligned with previous estimates (Prentice et al., 2011; Ciais et al., 2012). Other studies have found that this fertilization effect may be overestimated in the model (Kleinen et al., 2023; Dallmeyer et al., 2026), possibly because it lacks a component for soil nutrients limitation (Gier et al., 2024), or photosynthesis parameters may need an adjustment (Rogers et al., 2017). However, the exact cause remains unclear.

Since CO_2 is a well-mixed gas, CO_2 fertilization occurs globally and continuously during glacial cycles (Yang et al., 2022), but what we find in the LGC simulation is that it alone is not sufficient to predict changes in the terrestrial carbon budget everywhere. Only for "quasi-static" landscapes with small changes in vegetation (WC in Fig. 4a) can the CO_2 trajectory alone predict carbon accumulation on land, as well as the corresponding methane emissions (Fig. 5). This includes a large fraction of the tropics, where Lu et al. (2019) and Chen et al. (2019) also found CO_2 to be a good predictor of forest cover and the carbon sink, alongside temperature. However, also for the tropics some proxy data and simplified modelling found that hydroclimate changes are better predictors of the woody vegetation changes (Adam et al., 2021; Gosling et al., 2022). Rather than contradicting our results, this highlights the spatial complexity of the vegetation response, and demonstrates that a classification as shown in Fig. 4 can be useful to separate drivers.

For the regions where vegetation cover changes only slightly, the CO_2 fertilization effect is a dominant forcing and corresponding terrestrial fluxes are a function mainly of the prescribed CO_2 trajectory (Fig. 1b), rather than of internal model dynamics. Hence, the possibility of simulating fast (or abrupt) carbon transfers with the atmosphere from such places is largely dependent on input data in concentration-driven experiments like LGC or ICE. In other words, the variability pattern is fixed at the outset. The magnitude of the regional total, however, still depends on simulated vegetation percentages, which by definition in weakly changing regions amounts to changes of small amplitude.

4.2 Precession-paced biome shifts

In the case of highly variable ecotone-like regions, CO_2 fertilization by itself is not sufficient to predict the carbon cycle evolution and we must include the precession orbital cycle. Figures 2d and 2e already show the precession-paced dynamics that explain the carbon cycle fluctuations we observe in Fig. 5, at least for regions in the NH that are far from ice margins and change total vegetation drastically: there are slow fluctuations with a multi-millennial period whose phases of high carbon storage and high methane emissions coincide with warm isotopic stages. Precession controls not just the hydroclimate changes near the

https://doi.org/10.5194/egusphere-2026-5687
Preprint. Discussion started: 2 November 2026
© Author(s) 2026. CC BY 4.0 License.

tropics that modulate monsoon rainfall strength (Fig. 2d), but also the occurrence of favourable extra-tropical temperatures that promote boreal tree growth (Fig. 2e). Claussen et al. (2006) showed with a model of intermediate complexity how the vegetation response globally amplifies the precession signal during glacial cycles. Precession explains the biome reorganization leading to Sahara greening (Duque-Villegas et al., 2025) and the northeastern Siberian taiga-tundra boundary shift (Tian et al., 2018) depicted in Fig. 3. Meanwhile in the SH the orbital trends are anti-phased (see Fig. 1a), and it leads to carbon accumulation in SH subtropical deserts during (NH) cold isotopic stages (not shown).

Such multi-millennial scale variability in the global carbon cycle can also be seen in the global biomass results of Allen et al. (2020), who ran offline simulations with a land-carbon-only model. In a follow up study, Huntley et al. (2023) also found that global biomass for the last eight glacial cycles could be predicted with notable success using only atmospheric CO_2 and solstice insolation at 65° N (which also carries the precession signal). The amplitude of the terrestrial carbon variation (some 150 Pg C) also agrees with our results, although Huntley et al. (2023) show global values while we have selected only specific regions in the NH shown in Fig. 4a. Agreement with previous studies that used other Earth system models suggests that our results are not entirely model-dependent.

4.3 Fast meltwater-induced vegetation change

Not all variations in the terrestrial carbon cycle can be predicted using just CO_2 fertilization and orbital cycles. In Fig. 5 there are clear sub-millennial excursions that represent shifts in large amounts of land carbon and greatly impact methane emissions, appearing also as “outburst” GHG emissions to the atmosphere in Fig. 7. The connection to a weakening of North Atlantic circulation emerges from the study of the meltwater pulses preceding the Holocene in experiment LGC and the Heinrich-like events in the ICE experiments. The link provided by this mechanism is similar to the hydroclimate changes that explain the low-latitude reorganization of biomes at orbital pacing: a meltwater-induced sudden meridional displacement of tropical rainbands, which in turn affects monsoon moisture transport, as well as vegetation productivity and survival. Our finding that the ITCZ can be displaced briefly after North Atlantic cooling by about 1° also agrees with other models (McGee et al., 2018). The sudden ITCZ shift quickly turns the tropical NH into a fast source of terrestrial carbon, as suggested by proxy data (Legrain et al., 2024; Riddell-Young et al., 2025).

Whether the carbon released from land remains in the atmosphere depends not only on the effects of the AMOC weakening on marine biogeochemistry (Gottschalk et al., 2019), but also on the terrestrial response in the opposite hemisphere, as the AMOC changes can induce inter-hemispheric shifts in the ITCZ and associated tropical rain belts. Based on the BGC and ICE experiments, our results support the idea that during episodes of abrupt North Atlantic cooling, the NH land likely contributed sufficient GHG emissions to register centennial-scale jumps in atmospheric concentrations of GHGs in ice cores, both during the last deglaciation (Marcott et al., 2014) and the entire glacial period (Bauska et al., 2021). Indeed, Fig. 6a shows that first the land releases carbon (some of which the ocean draws down), and only later as NH vegetation recovers together with the AMOC, does the ocean release carbon as well. Figure 4 then highlights the most probable source regions according to our simulations.

https://doi.org/10.5194/egusphere-2026-5687
Preprint. Discussion started: 2 November 2026
© Author(s) 2026. CC BY 4.0 License.

4.4 Missing high-latitude land processes

A key limitation of our study is the lack of peat and permafrost formation modelling. Treat et al. (2019) and Müller and Joos (2020) demonstrated how peat accumulation and burial during past warm and cold phases of the last glacial cycle have a substantial impact on the global carbon cycle. In fact, a reconstruction of soil carbon by Lindgren et al. (2025) showed these cold carbon stocks were large enough to have a notable contribution to glacial–interglacial variations of atmospheric CO_2; therefore reducing the burden on ocean carbon outgassing during deglaciation phases. Because here we essentially focus on geographic and productivity changes in vegetation near the low latitudes, we must consider our results as providing only a conservative baseline for terrestrially sourced emissions of GHGs.

5 Conclusions

Explaining the variations during glacial cycles of trace GHG concentrations in ice-core data is still an outstanding challenge that is crucial for projecting plausible trajectories of a changing climate-carbon system. Here we present new transient simulations that, unlike previous research with low-dimensional or uncoupled model components, take advantage of a comprehensive Earth system model adapted for experiments over glacial cycles with a changing cryosphere. Our analyses focus on the impact of vegetation changes on the evolution of the global carbon and methane budgets over the last 130 000 years of the late Quaternary. The experiments together include not only dynamic climates and vegetation cover, but also interactively calculated ice sheets and atmospheric levels of CO_2 and CH_4. They reproduce realistic values that seem in reasonable agreement with proxy data and previous literature, although our performance assessment is mainly of a qualitative nature, since much other previous work elsewhere has evaluated the model we use.

We find that vegetation responses to past climate change contribute markedly to simulated variations of CO_2 and CH_4 concentrations in the atmosphere. A magnitude-based classification of vegetation cover variability helps us separate "quasi-static" and "highly dynamic" regions, which clearly accumulate carbon on land reservoirs at different rates during warm and cold periods, thereby interacting differently with the global carbon cycle. Quasi-static regions, predominantly within the tropics near the equator, change landscape vegetation only slightly, and it makes terrestrial carbon storage predictable from the CO_2 fertilization effect alone. Conversely, regions where vegetation cover changes drastically, like at the fringes of monsoon domains, follow a clear precession signal in carbon allocation, which also propagates to GHG emissions, and we can predict land carbon changes with a combination of CO_2 values and a precession-controlled orbital index. At a sub-orbital scale, we also find that fast vegetation responses, mainly within the low latitudes of the NH tropics, during meltwater-induced strong weakening of the North Atlantic circulation, can lead to fast jumps in simulated CO_2 and CH_4 levels. A similar mechanism of shifting hemispheric and monsoon rainbands underlies both precession-paced and meltwater-induced vegetation cover and productivity changes, and we can skilfully predict the subsequent variability in atmospheric GHG levels of terrestrial origin.

These findings can help to understand multi-centennial and multi-millennial signals in proxy records that may be otherwise difficult to explain from ocean biogeochemistry alone. Furthermore, they show that it is key to understand vegetation dynamics

https://doi.org/10.5194/egusphere-2026-5687
Preprint. Discussion started: 2 November 2026
© Author(s) 2026. CC BY 4.0 License.

over monsoon regions and biome transition zones, which are still difficult to represent in Earth system models and have persistent climate biases. According to our results, precession-meltwater-vegetation interactions need to be dynamically resolved in climate models to obtain plausible climate-carbon trajectories in future projections.

Code and data availability. The model source code of MPI-ESM1.2 is publicly available at https://doi.org/10.17617/3.H44EN5. Model output data and a post-processing Python package to reproduce our analyses are archived at https://doi.org/10.17617/3.NU4AHR. The data from Mikolajewicz et al. (2025) are publicly available at https://doi.org/10.26050/WDCC/PMMXMC1TDIr1142 and (https://doi.org/10.26050/WDCC/PMMXMC1TDIr1152. The Snyder (2016) data are in the supplementary material of https://doi.org/10.1038/nature19798. The Hoogakker et al. (2016) data are in the supplementary material of https://doi.org/10.5194/cp-12-51-2016. The Li et al. (2025) data are archived at https://doi.org/10.1594/PANGAEA.965907.

Author contributions. MDV, TK, and VB developed the research idea. MDV performed climate simulations, led the formal analysis and prepared a first draft of the manuscript. UM performed climate simulations. TK provided model code and input data. AD and MC contributed to the methodology and formal analysis. All authors discussed the results and participated in the writing of the final manuscript.

Competing interests. At least one of the (co-)author is a member of the editorial board of *Climate of the Past*. The authors have no other competing interests to declare.

Acknowledgements. We thank Thomas Riddick for constructive comments on an earlier version of the manuscript. We also thank Bo Liu for guidance on setting up the marine biogeochemistry run. This research is part of the "PalMod" project and has been supported by the Bundesministerium für Forschung, Technologie und Raumfahrt (BMFTR) under grant agreements No. 01LP2306A, 01LP1921A, and 01LP2306B. We used resources of the Deutsches Klimarechenzentrum (DKRZ) granted to us by its Scientific Steering Committee (WLA) under project ID bm1030. MDV, TK and VB are contributing to the Past to Future (P2F) project by the European Union's Horizon Europe research and innovation programme under grant agreement No. 101184070. AD is financed by PalMod Phase III (grant no. 01LP2306A) and by the "HESCOR" project funded by the program "Profilbildung 2022", an initiative of the Ministry of Culture and Science of the State of North-Rhine Westphalia, Germany (PB22-081).

https://doi.org/10.5194/egusphere-2026-5687
Preprint. Discussion started: 2 November 2026
© Author(s) 2026. CC BY 4.0 License.

References

Adam, M., Weitzel, N., and Rehfeld, K.: Identifying global-scale patterns of vegetation change during the last deglaciation from paleoclimate networks, Paleoceanography and Paleoclimatology, 36, 1–21, https://doi.org/10.1029/2021pa004265, 2021.

Adam, O., Bischoff, T., and Schneider, T.: Seasonal and interannual variations of the energy flux equator and ITCZ. Part I: Zonally averaged ITCZ position, Journal of Climate, 29, 3219–3230, https://doi.org/10.1175/jcli-d-15-0512.1, 2016.

Ainsworth, E. A. and Long, S. P.: What have we learned from 15 years of free-air CO2 enrichment (FACE)? A meta-analytic review of the responses of photosynthesis, canopy properties and plant production to rising CO2, New Phytologist, 165, 351–372, https://doi.org/10.1111/j.1469-8137.2004.01224.x, 2005.

Allen, J. R. M., Forrest, M., Hickler, T., Singarayer, J. S., Valdes, P. J., and Huntley, B.: Global vegetation patterns of the past 140,000 years, Journal of Biogeography, 47, 2073–2090, https://doi.org/10.1111/jbi.13930, 2020.

Arakawa, A. and Lamb, V. R.: Computational design of the basic dynamical processes of the UCLA general circulation model, Methods in Computational Physics: Advances in Research and Applications, 17, 173–265, https://doi.org/10.1016/b978-0-12-460817-7.50009-4, 1977.

Bauska, T. K., Marcott, S. A., and Brook, E. J.: Abrupt changes in the global carbon cycle during the last glacial period, Nature Geoscience, 14, 91–96, https://doi.org/10.1038/s41561-020-00680-2, 2021.

Berger, A.: Long-term variations of daily insolation and Quaternary climatic changes, Journal of the Atmospheric Sciences, 35, 2362–2367, https://doi.org/10.1175/1520-0469(1978)035<2362:LTVODI>2.0.CO;2, 1978.

Bouttes, N., Lhardy, F., Quiquet, A., Paillard, D., Goosse, H., and Roche, D. M.: Deglacial climate changes as forced by different ice sheet reconstructions, Climate of the Past, 19, 1027–1042, https://doi.org/10.5194/cp-19-1027-2023, 2023.

Briggs, R. D., Pollard, D., and Tarasov, L.: A data-constrained large ensemble analysis of Antarctic evolution since the Eemian, Quaternary Science Reviews, 103, 91–115, https://doi.org/10.1016/j.quascirev.2014.09.003, 2014.

Brovkin, V., Brücher, T., Kleinen, T., Zaehle, S., Joos, F., Roth, R., Spahni, R., Schmitt, J., Fischer, H., Leuenberger, M., Stone, E. J., Ridgwell, A., Chappellaz, J., Kehrwald, N., Barbante, C., Blunier, T., and Dahl Jensen, D.: Comparative carbon cycle dynamics of the present and last interglacial, Quaternary Science Reviews, 137, 15–32, https://doi.org/10.1016/j.quascirev.2016.01.028, 2016.

Brovkin, V., Lorenz, S., Raddatz, T., Ilyina, T., Stemmler, I., Toohey, M., and Claussen, M.: What was the source of the atmospheric CO_2 increase during the Holocene?, Biogeosciences, 16, 2543–2555, https://doi.org/10.5194/bg-16-2543-2019, 2019.

Chen, W., Zhu, D., Ciais, P., Huang, C., Viovy, N., and Kageyama, M.: Response of vegetation cover to CO2 and climate changes between Last Glacial Maximum and pre-industrial period in a dynamic global vegetation model, Quaternary Science Reviews, 218, 293–305, https://doi.org/10.1016/j.quascirev.2019.06.003, 2019.

Cheng, H., Edwards, R. L., Sinha, A., Spötl, C., Yi, L., Chen, S., Kelly, M., Kathayat, G., Wang, X., Li, X., Kong, X., Wang, Y., Ning, Y., and Zhang, H.: The Asian monsoon over the past 640,000 years and ice age terminations, Nature, 534, 640–646, https://doi.org/10.1038/nature18591, 2016.

Ciais, P., Tagliabue, A., Cuntz, M., Bopp, L., Scholze, M., Hoffmann, G., Lourantou, A., Harrison, S. P., Prentice, I. C., Kelley, D. I., Koven, C., and Piao, S. L.: Large inert carbon pool in the terrestrial biosphere during the Last Glacial Maximum, Nature Geoscience, 5, 74–79, https://doi.org/10.1038/ngeo1324, 2012.

Claussen, M., Fohlmeister, J., Ganopolski, A., and Brovkin, V.: Vegetation dynamics amplifies precessional forcing, Geophysical Research Letters, 33, 1–4, https://doi.org/10.1029/2006gl026111, 2006.

https://doi.org/10.5194/egusphere-2026-5687
Preprint. Discussion started: 2 November 2026
© Author(s) 2026. CC BY 4.0 License.



Claussen, M., Selent, K., Brovkin, V., Raddatz, T., and Gayler, V.: Impact of CO_2 and climate on Last Glacial maximum vegetation – a factor separation, Biogeosciences, 10, 3593–3604, https://doi.org/10.5194/bg-10-3593-2013, 2013.

Cruz, F. W., Burns, S. J., Karmann, I., Sharp, W. D., Vuille, M., Cardoso, A. O., Ferrari, J. A., Silva Dias, P. L., and Viana, O.: Insolation-driven changes in atmospheric circulation over the past 116,000 years in subtropical Brazil, Nature, 434, 63–66, https://doi.org/10.1038/nature03365, 2005.

Dallmeyer, A., Claussen, M., and Brovkin, V.: Harmonising plant functional type distributions for evaluating Earth system models, Climate of the Past, 15, 335–366, https://doi.org/10.5194/cp-15-335-2019, 2019.

Dallmeyer, A., Kleinen, T., Claussen, M., Weitzel, N., Cao, X., and Herzschuh, U.: The deglacial forest conundrum, Nature Communications, 13, 1–10, https://doi.org/10.1038/s41467-022-33646-6, 2022.

Dallmeyer, A., Weitzel, N., Schild, L., Herzschuh, U., Kleinen, T., and Claussen, M.: Unravelling the tree cover dynamics over the last 20000 years on the Northern Hemisphere, Climate of the Past, 22, 1125–1157, https://doi.org/10.5194/cp-22-1125-2026, 2026.

Davies-Barnard, T., Ridgwell, A., Singarayer, J., and Valdes, P.: Quantifying the influence of the terrestrial biosphere on glacial–interglacial climate dynamics, Climate of the Past, 13, 1381–1401, https://doi.org/10.5194/cp-13-1381-2017, 2017.

Duque-Villegas, M., Claussen, M., Brovkin, V., and Kleinen, T.: Effects of orbital forcing, greenhouse gases and ice sheets on Saharan greening in past and future multi-millennia, Climate of the Past, 18, 1897–1914, https://doi.org/10.5194/cp-18-1897-2022, 2022.

Duque-Villegas, M., Claussen, M., Kleinen, T., Bader, J., and Reick, C. H.: Pattern scaling of simulated vegetation change in northern Africa during glacial cycles, Climate of the Past, 21, 773–794, https://doi.org/10.5194/cp-21-773-2025, 2025.

Extier, T., Six, K. D., Liu, B., Paulsen, H., and Ilyina, T.: Local oceanic CO2 outgassing triggered by terrestrial carbon fluxes during deglacial flooding, Climate of the Past, 18, 273–292, https://doi.org/10.5194/cp-18-273-2022, 2022.

Fastovich, D., Meyers, S. R., Saupe, E. E., Williams, J. W., Dornelas, M., Dowding, E. M., Finnegan, S., Huang, H.-H. M., Jonkers, L., Kiessling, W., Kocsis, Á. T., Li, Q., Liow, L. H., Na, L., Penny, A. M., Pippenger, K., Renaudie, J., Rillo, M. C., Smith, J., Steinbauer, M. J., Sugawara, M., Tomašových, A., Yasuhara, M., and Hull, P. M.: Coupled, decoupled, and abrupt responses of vegetation to climate across timescales, Science, 389, 64–68, https://doi.org/10.1126/science.adr6700, 2025.

Ganopolski, A. and Brovkin, V.: Simulation of climate, ice sheets and CO2 evolution during the last four glacial cycles with an Earth system model of intermediate complexity, Climate of the Past, 13, 1695–1716, https://doi.org/10.5194/cp-13-1695-2017, 2017.

Gerhart, L. M. and Ward, J. K.: Plant responses to low CO2 of the past, New Phytologist, 188, 674–695, https://doi.org/10.1111/j.1469-8137.2010.03441.x, 2010.

Gier, B. K., Schlund, M., Friedlingstein, P., Jones, C. D., Jones, C., Zaehle, S., and Eyring, V.: Representation of the terrestrial carbon cycle in CMIP6, Biogeosciences, 21, 5321–5360, https://doi.org/10.5194/bg-21-5321-2024, 2024.

Gonzales, L. M. and Grimm, E. C.: Synchronization of late-glacial vegetation changes at Crystal Lake, Illinois, USA with the North Atlantic Event Stratigraphy, Quaternary Research, 72, 234–245, https://doi.org/10.1016/j.yqres.2009.05.001, 2009.

Gosling, W. D., Miller, C. S., Shanahan, T. M., Holden, P. B., Overpeck, J. T., and van Langevelde, F.: A stronger role for long-term moisture change than for CO2 in determining tropical woody vegetation change, Science, 376, 653–656, https://doi.org/10.1126/science.abg4618, 2022.

Gottschalk, J., Battaglia, G., Fischer, H., Frölicher, T. L., Jaccard, S. L., Jeltsch-Thömmes, A., Joos, F., Köhler, P., Meissner, K. J., Menviel, L., Nehrbass-Ahles, C., Schmitt, J., Schmittner, A., Skinner, L. C., and Stocker, T. F.: Mechanisms of millennial-scale atmospheric CO2 change in numerical model simulations, Quaternary Science Reviews, 220, 30–74, https://doi.org/10.1016/j.quascirev.2019.05.013, 2019.

https://doi.org/10.5194/egusphere-2026-5687
Preprint. Discussion started: 2 November 2026
© Author(s) 2026. CC BY 4.0 License.

Gowan, E. J., Zhang, X., Khosravi, S., Rovere, A., Stocchi, P., Hughes, A. L. C., Gyllencreutz, R., Mangerud, J., Svendsen, J.-I., and Lohmann, G.: A new global ice sheet reconstruction for the past 80000 years, Nature Communications, 12, 1–9, https://doi.org/10.1038/s41467-021-21469-w, 2021.

Harrison, S.: BIOME 6000 DB classified plotfile version 1, University of Reading, https://doi.org/http://dx.doi.org/10.17864/1947.99, 2017.

Harrison, S. P. and Prentice, C. I.: Climate and CO2 controls on global vegetation distribution at the last glacial maximum: analysis based on palaeovegetation data, biome modelling and palaeoclimate simulations, Global Change Biology, 9, 983–1004, https://doi.org/10.1046/j.1365-2486.2003.00640.x, 2003.

Harrison, S. P., Bartlein, P. J., Cruz-Silva, E., Haas, O., Jackson, S. T., Kaushal, N., Liu, M., Magri, D., Robson, D. T., Vettoretti, G., and Prentice, I. C.: Paleoclimate perspectives on contemporary climate change, Annual Review of Environment and Resources, 50, 67–95, https://doi.org/10.1146/annurev-environ-112922-110121, 2025.

Hibler, W. D.: A dynamic thermodynamic sea ice model, Journal of Physical Oceanography, 9, 815–846, https://doi.org/10.1175/1520-0485(1979)009<0815:adtsim>2.0.co;2, 1979.

Hoogakker, B. A. A., Smith, R. S., Singarayer, J. S., Marchant, R., Prentice, I. C., Allen, J. R. M., Anderson, R. S., Bhagwat, S. A., Behling, H., Borisova, O., Bush, M., Correa-Metrio, A., de Vernal, A., Finch, J. M., Fréchette, B., Lozano-Garcia, S., Gosling, W. D., Granoszewski, W., Grimm, E. C., Grüger, E., Hanselman, J., Harrison, S. P., Hill, T. R., Huntley, B., Jiménez-Moreno, G., Kershaw, P., Ledru, M.-P., Magri, D., McKenzie, M., Müller, U., Nakagawa, T., Novenko, E., Penny, D., Sadori, L., Scott, L., Stevenson, J., Valdes, P. J., Vandergoes, M., Velichko, A., Whitlock, C., and Tzedakis, C.: Terrestrial biosphere changes over the last 120 kyr, Climate of the Past, 12, 51–73, https://doi.org/10.5194/cp-12-51-2016, 2016.

Huntley, B., Allen, J. R. M., Forrest, M., Hickler, T., Ohlemüller, R., Singarayer, J. S., and Valdes, P. J.: Global biome patterns of the middle and late Pleistocene, Journal of Biogeography, 50, 1352–1372, https://doi.org/10.1111/jbi.14619, 2023.

Ilyina, T., Six, K. D., Segschneider, J., Maier-Reimer, E., Li, H., and Núñez-Riboni, I.: Global ocean biogeochemistry model HAMOCC: Model architecture and performance as component of the MPI-Earth system model in different CMIP5 experimental realizations, Journal of Advances in Modeling Earth Systems, 5, 287–315, https://doi.org/10.1029/2012ms000178, 2013.

Jeltsch-Thömmes, A., Battaglia, G., Cartapanis, O., Jaccard, S. L., and Joos, F.: Low terrestrial carbon storage at the Last Glacial Maximum: constraints from multi-proxy data, Climate of the Past, 15, 849–879, https://doi.org/10.5194/cp-15-849-2019, 2019.

Jungclaus, J. H., Fischer, N., Haak, H., Lohmann, K., Marotzke, J., Matei, D., Mikolajewicz, U., Notz, D., and von Storch, J. S.: Characteristics of the ocean simulations in the Max Planck Institute Ocean Model (MPIOM) the ocean component of the MPI-Earth system model, Journal of Advances in Modeling Earth Systems, 5, 422–446, https://doi.org/10.1002/jame.20023, 2013.

Kapsch, M.-L., Mikolajewicz, U., Ziemen, F., and Schannwell, C.: Ocean response in transient simulations of the last deglaciation dominated by underlying ice-sheet reconstruction and method of meltwater distribution, Geophysical Research Letters, 49, 1–11, https://doi.org/10.1029/2021gl096767, 2022.

Kinne, S., O'Donnel, D., Stier, P., Kloster, S., Zhang, K., Schmidt, H., Rast, S., Giorgetta, M., Eck, T. F., and Stevens, B.: MAC-v1: A new global aerosol climatology for climate studies, Journal of Advances in Modeling Earth Systems, 5, 704–740, https://doi.org/10.1002/jame.20035, 2013.

Kleinen, T., Mikolajewicz, U., and Brovkin, V.: Terrestrial methane emissions from the Last Glacial Maximum to the preindustrial period, Climate of the Past, 16, 575–595, https://doi.org/10.5194/cp-16-575-2020, 2020.

Kleinen, T., Gromov, S., Steil, B., and Brovkin, V.: Atmospheric methane since the last glacial maximum was driven by wetland sources, Climate of the Past, 19, 1081–1099, https://doi.org/10.5194/cp-19-1081-2023, 2023.

https://doi.org/10.5194/egusphere-2026-5687
Preprint. Discussion started: 2 November 2026
© Author(s) 2026. CC BY 4.0 License.

Kobayashi, H., Oka, A., Obase, T., and Abe-Ouchi, A.: Assessing transient changes in the ocean carbon cycle during the last deglaciation through carbon isotope modeling, Climate of the Past, 20, 769–787, https://doi.org/10.5194/cp-20-769-2024, 2024.

Köhler, P., Nehrbass-Ahles, C., Schmitt, J., Stocker, T. F., and Fischer, H.: A 156 kyr smoothed history of the atmospheric greenhouse gases CO2, CH4, and N2O and their radiative forcing, Earth System Science Data, 9, 363–387, https://doi.org/10.5194/essd-9-363-2017, 2017.

Körner, C.: Plant CO2 responses: an issue of definition, time and resource supply, New Phytologist, 172, 393–411, https://doi.org/10.1111/j.1469-8137.2006.01886.x, 2006.

Koutsodendris, A., Dakos, V., Fletcher, W. J., Knipping, M., Kotthoff, U., Milner, A. M., Müller, U. C., Kaboth-Bahr, S., Kern, O. A., Kolb, L., Vakhrameeva, P., Wulf, S., Christanis, K., Schmiedl, G., and Pross, J.: Atmospheric CO2 forcing on Mediterranean biomes during the past 500 kyrs, Nature Communications, 14, 1–12, https://doi.org/10.1038/s41467-023-37388-x, 2023.

Lawman, A. E., Sun, C., Wu, X., Sun, T., Piatrunia, N., Gomez, K., Kageyama, M., Merkel, U., Prange, M., Otto-Bliesner, B., Zhang, X., DiNezio, P., and Shanahan, T.: Mechanisms driving the global tropical response to a weakened AMOC during Heinrich Stadial 1, Quaternary Science Reviews, 369, 109 567, https://doi.org/10.1016/j.quascirev.2025.109567, 2025.

Legrain, E., Capron, E., Menviel, L., Wohleber, A., Parrenin, F., Teste, G., Landais, A., Bouchet, M., Grilli, R., Nehrbass-Ahles, C., Silva, L., Fischer, H., and Stocker, T. F.: Centennial-scale variations in the carbon cycle enhanced by high obliquity, Nature Geoscience, 17, 1154–1161, https://doi.org/10.1038/s41561-024-01556-5, 2024.

Li, C., Dallmeyer, A., Ni, J., Chevalier, M., Willeit, M., Andreev, A. A., Cao, X., Schild, L., Heim, B., and Herzschuh, U.: Global biome changes over the last 21,000 years inferred from model-data comparisons, Climate of the Past, pp. 1001–1024, https://doi.org/10.5194/cp-21-1001-2025, 2025.

Lindgren, A., Kuhry, P., Holloway, M., Lu, Z., Tanski, G., and Hugelius, G.: Massive losses and gains of northern land carbon stocks since the Last Glacial Maximum, Science Advances, 11, 1–11, https://doi.org/10.1126/sciadv.adt6231, 2025.

Liu, B., Maerz, J., and Ilyina, T.: Glacial Atlantic carbon storage enhanced by a shallow AMOC and marine aggregates sinking, Geophysical Research Letters, 51, 1–15, https://doi.org/10.1029/2024gl109736, 2024.

Liu, J., Wang, B., Ding, Q., Kuang, X., Soon, W., and Zorita, E.: Centennial variations of the global monsoon precipitation in the last millennium: results from ECHO-G model, Journal of Climate, 22, 2356–2371, https://doi.org/10.1175/2008jcli2353.1, 2009.

Lu, Z., Miller, P. A., Zhang, Q., Wårlind, D., Nieradzik, L., Sjolte, J., Li, Q., and Smith, B.: Vegetation pattern and terrestrial carbon variation in past warm and cold climates, Geophysical Research Letters, 46, 8133–8143, https://doi.org/10.1029/2019gl083729, 2019.

Marcott, S. A., Bauska, T. K., Buizert, C., Steig, E. J., Rosen, J. L., Cuffey, K. M., Fudge, T. J., Severinghaus, J. P., Ahn, J., Kalk, M. L., McConnell, J. R., Sowers, T., Taylor, K. C., White, J. W. C., and Brook, E. J.: Centennial-scale changes in the global carbon cycle during the last deglaciation, Nature, 514, 616–619, https://doi.org/10.1038/nature13799, 2014.

Mauritsen, T., Bader, J., Becker, T., Behrens, J., Bittner, M., Brokopf, R., Brovkin, V., Claussen, M., Crueger, T., Esch, M., Fast, I., Fiedler, S., Fläschner, D., Gayler, V., Giorgetta, M., Goll, D. S., Haak, H., Hagemann, S., Hedemann, C., Hohenegger, C., Ilyina, T., Jahns, T., Jimenéz-de-la Cuesta, D., Jungclaus, J., Kleinen, T., Kloster, S., Kracher, D., Kinne, S., Kleberg, D., Lasslop, G., Kornblueh, L., Marotzke, J., Matei, D., Meraner, K., Mikolajewicz, U., Modali, K., Möbis, B., Müller, W. A., Nabel, J. E. M. S., Nam, C. C. W., Notz, D., Nyawira, S., Paulsen, H., Peters, K., Pincus, R., Pohlmann, H., Pongratz, J., Popp, M., Raddatz, T. J., Rast, S., Redler, R., Reick, C. H., Rohrschneider, T., Schemann, V., Schmidt, H., Schnur, R., Schulzweida, U., Six, K. D., Stein, L., Stemmler, I., Stevens, B., Storch, J. v., Tian, F., Voigt, A., Vrese, P., Wieners, K., Wilkenskjeld, S., Winkler, A., and Roeckner, E.: Developments in the MPI-M Earth System Model version 1.2 (MPI-ESM1.2) and its response to increasing CO2, Journal of Advances in Modeling Earth Systems, 11, 998–1038, https://doi.org/10.1029/2018MS001400, 2019.

https://doi.org/10.5194/egusphere-2026-5687
Preprint. Discussion started: 2 November 2026
© Author(s) 2026. CC BY 4.0 License.

McGee, D., Moreno-Chamarro, E., Green, B., Marshall, J., Galbraith, E., and Bradtmiller, L.: Hemispherically asymmetric trade wind changes as signatures of past ITCZ shifts, Quaternary Science Reviews, 180, 214–228, https://doi.org/10.1016/j.quascirev.2017.11.020, 2018.

Meccia, V. L. and Mikolajewicz, U.: Interactive ocean bathymetry and coastlines for simulating the last deglaciation with the Max Planck Institute Earth System Model (MPI-ESM-v1. 2), Geoscientific Model Development, 11, 4677–4692, https://doi.org/10.5194/gmd-11-4677-2018, 2018.

Menviel, L., Govin, A., Avenas, A., Meissner, K. J., Grant, K. M., and Tzedakis, P. C.: Drivers of the evolution and amplitude of African Humid Periods, Communications Earth & Environment, 2, 1–11, https://doi.org/10.1038/s43247-021-00309-1, 2021.

Mikolajewicz, U., Ziemen, F., Cioni, G., Claussen, M., Fraedrich, K. F., Heidkamp, M., Hohenegger, C., de la Cuesta, D. J., Kapsch, M.-L., Lemburg, A., Mauritsen, T., Meraner, K., Röber, N., Schmidt, H., Six, K. D., Stemmler, I., Tamarin-Brodsky, T., Winkler, A., Zhu, X., and Stevens, B.: The climate of a retrograde rotating Earth, Earth System Dynamics, 9, 1191–1215, https://doi.org/10.5194/esd-9-1191-2018, 2018.

Mikolajewicz, U., Kapsch, M.-L., Schannwell, C., Six, K. D., Ziemen, F. A., Bagge, M., Baudouin, J.-P., Erokhina, O., Gayler, V., Klemann, V., Meccia, V. L., Mouchet, A., and Riddick, T.: Deglaciation and abrupt events in a coupled comprehensive atmosphere–ocean–ice-sheet–solid-earth model, Climate of the Past, 21, 719–751, https://doi.org/10.5194/cp-21-719-2025, 2025.

Müller, J. and Joos, F.: Global peatland area and carbon dynamics from the Last Glacial Maximum to the present – a process-based model investigation, Biogeosciences, 17, 5285–5308, https://doi.org/10.5194/bg-17-5285-2020, 2020.

Nolan, C., Overpeck, J. T., Allen, J. R. M., Anderson, P. M., Betancourt, J. L., Binney, H. A., Brewer, S., Bush, M. B., Chase, B. M., Cheddadi, R., Djamali, M., Dodson, J., Edwards, M. E., Gosling, W. D., Haberle, S., Hotchkiss, S. C., Huntley, B., Ivory, S. J., Kershaw, A. P., Kim, S.-H., Latorre, C., Leydet, M., Lézine, A.-M., Liu, K.-B., Liu, Y., Lozhkin, A. V., McGlone, M. S., Marchant, R. A., Momohara, A., Moreno, P. I., Müller, S., Otto-Bliesner, B. L., Shen, C., Stevenson, J., Takahara, H., Tarasov, P. E., Tipton, J., Vincens, A., Weng, C., Xu, Q., Zheng, Z., and Jackson, S. T.: Past and future global transformation of terrestrial ecosystems under climate change, Science, 361, 920–923, https://doi.org/10.1126/science.aan5360, 2018.

Osman, M. B., Tierney, J. E., Zhu, J., Tardif, R., Hakim, G. J., King, J., and Poulsen, C. J.: Globally resolved surface temperatures since the Last Glacial Maximum, Nature, 599, 239–244, https://doi.org/10.1038/s41586-021-03984-4, 2021.

Overpeck, J. T., Webb, T., and Prentice, I. C.: Quantitative interpretation of fossil pollen spectra: dissimilarity coefficients and the method of modern analogs, Quaternary Research, 23, 87–108, https://doi.org/10.1016/0033-5894(85)90074-2, 1985.

Paulsen, H., Ilyina, T., Six, K. D., and Stemmler, I.: Incorporating a prognostic representation of marine nitrogen fixers into the global ocean biogeochemical model HAMOCC, Journal of Advances in Modeling Earth Systems, 9, 438–464, https://doi.org/10.1002/2016ms000737, 2017.

Peltier, W. R., Argus, D. F., and Drummond, R.: Space geodesy constrains ice age terminal deglaciation: the global ICE-6G_C (VM5a) model, Journal of Geophysical Research: Solid Earth, 120, 450–487, https://doi.org/10.1002/2014jb011176, 2015.

Prentice, I. C., Bartlein, P. J., and Webb, T.: Vegetation and climate change in eastern North America since the Last Glacial Maximum, Ecology, 72, 2038–2056, https://doi.org/10.2307/1941558, 1991.

Prentice, I. C., Harrison, S. P., and Bartlein, P. J.: Global vegetation and terrestrial carbon cycle changes after the last ice age, New Phytologist, 189, 988–998, https://doi.org/10.1111/j.1469-8137.2010.03620.x, 2011.

https://doi.org/10.5194/egusphere-2026-5687
Preprint. Discussion started: 2 November 2026
© Author(s) 2026. CC BY 4.0 License.

Railsback, L. B., Gibbard, P. L., Head, M. J., Voarintsoa, N. R. G., and Toucanne, S.: An optimized scheme of lettered marine isotope substages for the last 1.0 million years, and the climatostratigraphic nature of isotope stages and substages, Quaternary Science Reviews, 111, 94–106, https://doi.org/10.1016/j.quascirev.2015.01.012, 2015.

Reick, C. H., Raddatz, T., Brovkin, V., and Gayler, V.: Representation of natural and anthropogenic land cover change in MPI-ESM, Journal of Advances in Modeling Earth Systems, 5, 459–482, https://doi.org/10.1002/jame.20022, 2013.

Reick, C. H., Gayler, V., Goll, D., Hagemann, S., Heidkamp, M., Nabel, J. E. M. S., Raddatz, T., Roeckner, E., Schnur, R., and Wilkenskjeld, S.: JSBACH 3 - The land component of the MPI Earth System Model: documentation of version 3.2, vol. 240 of *Berichte zur Erdystemforschung*, Max Planck Institute for Meteorology, Hamburg, Germany, https://doi.org/10.17617/2.3279802, 2021.

Riddell-Young, B., Rosen, J., Brook, E., Buizert, C., Martin, K., Lee, J., Edwards, J., Mühl, M., Schmitt, J., Fischer, H., and Blunier, T.: Atmospheric methane variability through the Last Glacial Maximum and deglaciation mainly controlled by tropical sources, Nature Geoscience, 16, 1174–1180, https://doi.org/10.1038/s41561-023-01332-x, 2023.

Riddell-Young, B., Lee, J. E., Brook, E. J., Schmitt, J., Fischer, H., Bauska, T. K., Menking, J. A., Iseli, R., and Clark, J. R.: Abrupt changes in biomass burning during the last glacial period, Nature, 637, 91–96, https://doi.org/10.1038/s41586-024-08363-3, 2025.

Riddick, T., Brovkin, V., Hagemann, S., and Mikolajewicz, U.: Dynamic hydrological discharge modelling for coupled climate model simulations of the last glacial cycle: the MPI-DynamicHD model version 3.0, Geoscientific Model Development, 11, 4291–4316, https://doi.org/10.5194/gmd-11-4291-2018, 2018.

Rogers, A., Medlyn, B. E., Dukes, J. S., Bonan, G., von Caemmerer, S., Dietze, M. C., Kattge, J., Leakey, A. D. B., Mercado, L. M., Niinemets, Ü., Prentice, I. C., Serbin, S. P., Sitch, S., Way, D. A., and Zaehle, S.: A roadmap for improving the representation of photosynthesis in Earth system models, New Phytologist, 213, 22–42, https://doi.org/10.1111/nph.14283, 2017.

Ronge, T. A., Frische, M., Fietzke, J., Stephens, A. L., Bostock, H., and Tiedemann, R.: Southern Ocean contribution to both steps in deglacial atmospheric CO2 rise, Scientific Reports, 11, https://doi.org/10.1038/s41598-021-01657-w, 2021.

Rossignol-Strick, M.: African monsoons, an immediate climate response to orbital insolation, Nature, 304, 46–49, https://doi.org/10.1038/304046a0, 1983.

Sánchez Goñi, M. F., Desprat, S., Fletcher, W. J., Morales-Molino, C., Naughton, F., Oliveira, D., Urrego, D. H., and Zorzi, C.: Pollen from the deep-sea: a breakthrough in the mystery of the ice ages, Frontiers in Plant Science, 9, 1–24, https://doi.org/10.3389/fpls.2018.00038, 2018.

Schannwell, C., Mikolajewicz, U., Kapsch, M.-L., and Ziemen, F.: A mechanism for reconciling the synchronisation of Heinrich events and Dansgaard-Oeschger cycles, Nature Communications, 15, 1–8, https://doi.org/10.1038/s41467-024-47141-7, 2024.

Schindlbeck-Belo, J. C., Toohey, M., Jegen, M., Kutterolf, S., and Rehfeld, K.: PalVol v1: a proxy-based semi-stochastic ensemble reconstruction of volcanic stratospheric sulfur injection for the last glacial cycle (140 000–50 BP), Earth System Science Data, 16, 1063–1081, https://doi.org/10.5194/essd-16-1063-2024, 2024.

Shuman, B. N., Newby, P., and Donnelly, J. P.: Abrupt climate change as an important agent of ecological change in the Northeast U.S. throughout the past 15,000 years, Quaternary Science Reviews, 28, 1693–1709, https://doi.org/10.1016/j.quascirev.2009.04.005, 2009.

Simpson, G. L.: Modelling palaeoecological time series using generalised additive models, Frontiers in Ecology and Evolution, 6, 1–21, https://doi.org/10.3389/fevo.2018.00149, 2018.

Skinner, L. C., Fallon, S., Waelbroeck, C., Michel, E., and Barker, S.: Ventilation of the deep Southern Ocean and deglacial CO2 rise, Science, 328, 1147–1151, https://doi.org/10.1126/science.1183627, 2010.

https://doi.org/10.5194/egusphere-2026-5687
Preprint. Discussion started: 2 November 2026
© Author(s) 2026. CC BY 4.0 License.

Snyder, C. W.: Evolution of global temperature over the past two million years, Nature, 538, 226–228, https://doi.org/10.1038/nature19798, 2016.

Stevens, B., Giorgetta, M., Esch, M., Mauritsen, T., Crueger, T., Rast, S., Salzmann, M., Schmidt, H., Bader, J., Block, K., Brokopf, R., Fast, I., Kinne, S., Kornblueh, L., Lohmann, U., Pincus, R., Reichler, T., and Roeckner, E.: Atmospheric component of the MPI-M Earth system model: ECHAM6, Journal of Advances in Modeling Earth Systems, 5, 146–172, https://doi.org/10.1002/jame.20015, 2013.

Svenning, J.-C. and Sandel, B.: Disequilibrium vegetation dynamics under future climate change, American Journal of Botany, 100, 1266–1286, https://doi.org/10.3732/ajb.1200469, 2013.

Tarasov, L., Dyke, A. S., Neal, R. M., and Peltier, W. R.: A data-calibrated distribution of deglacial chronologies for the North American ice complex from glaciological modeling, Earth and Planetary Science Letters, 315, 30–40, https://doi.org/10.1016/j.epsl.2011.09.010, 2012.

Tian, F., Cao, X., Dallmeyer, A., Lohmann, G., Zhang, X., Ni, J., Andreev, A., Anderson, P. M., Lozhkin, A. V., Bezrukova, E., Rudaya, N., Xu, Q., and Herzschuh, U.: Biome changes and their inferred climatic drivers in northern and eastern continental Asia at selected times since 40 cal ka BP, Vegetation History and Archaeobotany, 27, 365–379, https://doi.org/10.1007/s00334-017-0653-8, 2018.

Tierney, J. E., Zhu, J., King, J., Malevich, S. B., Hakim, G. J., and Poulsen, C. J.: Glacial cooling and climate sensitivity revisited, Nature, 584, 569–573, https://doi.org/10.1038/s41586-020-2617-x, 2020.

Treat, C. C., Kleinen, T., Broothaerts, N., Dalton, A. S., Dommain, R., Douglas, T. A., Drexler, J. Z., Finkelstein, S. A., Grosse, G., Hope, G., Hutchings, J., Jones, M. C., Kuhry, P., Lacourse, T., Lähteenoja, O., Loisel, J., Notebaert, B., Payne, R. J., Peteet, D. M., Sannel, A. B. K., Stelling, J. M., Strauss, J., Swindles, G. T., Talbot, J., Tarnocai, C., Verstraeten, G., Williams, C. J., Xia, Z., Yu, Z., Väliranta, M., Hättestrand, M., Alexanderson, H., and Brovkin, V.: Widespread global peatland establishment and persistence over the last 130,000 y, Proceedings of the National Academy of Sciences, 116, 4822–4827, https://doi.org/10.1073/pnas.1813305116, 2019.

Williams, J. W., Blois, J. L., and Shuman, B. N.: Extrinsic and intrinsic forcing of abrupt ecological change: case studies from the late Quaternary, Journal of Ecology, 99, 664–677, https://doi.org/10.1111/j.1365-2745.2011.01810.x, 2011.

Yang, J.-W., Brandon, M., Landais, A., Duchamp-Alphonse, S., Blunier, T., Prié, F., and Extier, T.: Global biosphere primary productivity changes during the past eight glacial cycles, Science, 375, 1145–1151, https://doi.org/10.1126/science.abj8826, 2022.